Photocatalytic Hydrogen Production: A Rift into the Future Energy Supply

Konstantinos C. Christoforidis[a, b] and Paolo Fornasiero*[a]

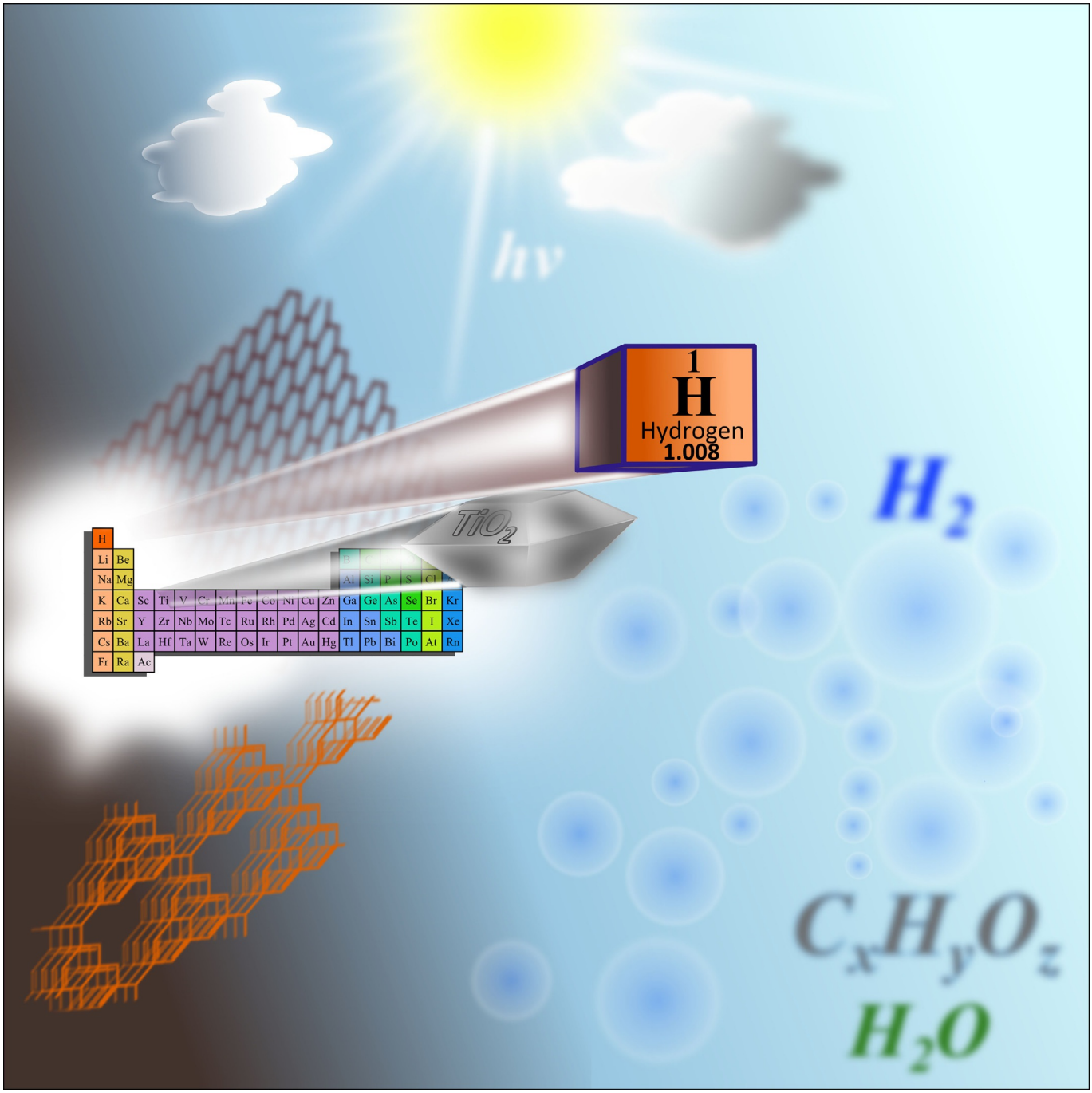

Photocatalytic hydrogen (H_2) production is a process that converts solar energy into chemical energy by means of a suitable photocatalyst. After the huge amount of systems that have been tested in the last forty years, the advent of nanotechnology and a careful design at molecular level, allow to obtain attractive activity, even using pure visible light. At the same time we are approaching reasonable photocatalyst stability in laboratory test, and the attention is paid to identify cost-effective photocatalysts that might find real applications. This Review provides a broad overview of the elementary steps of the heterogeneous photocatalytic H_2 production, including an outline of the physico-chemical reactions occurring on semiconductors and cocatalysts. The use of different renewable oxygenates as sustainable sacrificial agent for the H_2 production is outlined, in view of a transition from fossil fuels to pure water splitting. Finally, the recent advances in the development of photocatalyst are discussed focusing on the current progress in organic and hybrid organic/inorganic photocatalysts.

1. Introduction

Nowadays, one of the main technological challenges that we are facing is the ability to provide a sustainable supply of clean energy. Over the last decades the world energy consumption has been grown exponentially. This, together with the progressive depletion of fossil fuels reserves and the negative environmental impact of their use make indispensable the development of technologies for energy production based on renewable resources. Among all possible options, the largest renewable energy resource is provided by the sun. The average daily energy provided by the sun (10^{22} J) covers by far the global annual current demands for energy.[1] Therefore, solar energy presents the greatest potential to meet the future energy demands under the rules of sustainability. Thus, the exploitation of solar energy seems suitable both to cover energy demands in the future and overcome environmental related issues originating from the traditional energy production processes based on fossil fuels.

The need to harvest and convert solar energy into an appropriate energy form (electricity, chemicals, or fuels) has triggered intensive research in this field. Over the last decades different strategies have been developed. The photovoltaic cell technology converts solar energy into electrical energy. It is a commercialized process and the efficiency has been increased significantly over the last years, exceeding the significant value of 20%. However, despite major improvements in smart grids and new batteries, large scale energy storage remains a major limitation. On the contrary, converting solar energy into chemical energy producing renewable fuels, the so called "solar fuels", provides obvious advantages for practical applications. In this regard, the direct conversion of solar energy to chemical energy can be performed through two different routes: a) CO_2 reduction into hydrocarbons (e.g. methane, methanol, ethanol etc.) and b) H_2 generation.

H_2, a carbon-free fuel, is potentially an ideal energy carrier. When combined with O_2 in a Fuel Cell (FC), the chemical energy stored in the H–H bond is released producing water only. However, before the World can face a new energy scenario, there are several issues that must be solved. Amongst them, the realization of an efficient H_2 production process that meets industrial needs is the most crucial step. Ideally, such method must take into account a long-term supply of the H_2 source, environmental aspects such as minimization or elimination of any waste products with particular attention to CO_2 or any other greenhouse gas (GHG). A variety of process technologies have been proposed so far including thermal chemical, chemical, biological, electrolytic, photoelectrolytic, and photocatalytic processes. These processes make use of carbon feedstocks (fossil fuels, biomass, wastes) or water as H-source.[2] Currently, the vast majority of H_2 is produced from natural gas through the steam reforming of methane (SRM), a process which is followed by the water-gas shift reaction (WGS) making use of the produced CO in the first step to maximize H_2 production.[3] However, this approach cannot be considered sustainable owing to the limited availability of fossil fuels and the production of CO_2, a major GHG that contributes to the global warming. Most of the methods mentioned above require high pressures and temperatures, the application of an external bias or the use of non-renewable H_2 source. Amongst them, photoassisted processes making use of solar irradiation and H_2O or potentially renewable feedstocks present obvious advantages and have gained significant attention over the last years. Recent studies have shown that H_2 production using solar light driven approaches are potentially competitive compared to conventional methodologies based on non-renewable resources.[4]

Since the pioneering work of Honda and Fujishima in 1972 which demonstrated photoassisted electrochemical water splitting (WS) into H_2 and O_2,[5] various approaches and photocatalysts have been applied for solar light driven catalytic H_2 production. Among these methods, photocatalytic H_2 production from water, operating under ambient conditions (pressure, temperature), is the most attractive and challenging. This approach correspond to a stand-alone process that harvests and

[a] *Dr. K. C. Christoforidis, Prof. Dr. P. Fornasiero*
Department of Chemical and Pharmaceutical Sciences
ICCOM-CNR and INSTM
University of Trieste
via L.Giorgieri 1, 34127, Trieste (Italy)
E-mail: pfornasiero@units.it

[b] *Dr. K. C. Christoforidis*
Department of Chemical Engineering
Imperial College London
South Kensington Campus, London SW7 2AZ (UK)

The ORCID identification number(s) for the author(s) of this article can be found under http://dx.doi.org/10.1002/cctc.201601659.

stores solar energy into chemical energy. As an alternative process to pure WS, photoreforming makes use of oxygenated organic substrates and solar energy. In this case, when bio-available oxygenates are used as sacrificial agents, the method is considered to be close to a carbon-neutral process since the produced CO_2 can be converted again into biomass through plant photosynthesis. The entire sustainability strongly depends on the origin of the organic substrate, i.e. non sustainable first generation biomasses or attractive second/next generation biomasses.[6]

The photocatalytic H_2 production process from WS consists of two half reactions: the proton reduction and the highly demanding 4-electron water oxidation. In the photoreforming process, oxidation of the organic substrate takes place instead. The organic substrate serves also as a proton source. Therefore, it can be considered as the coupling of the oxidation of an organic substance and proton reduction.[7] The fundamental reactions are given in the following Equations (1)–(4) and are summarized in Figure 1.

$$2\,H^+ + 2e^- \rightarrow H_2 \qquad \text{Reduction half reaction} \qquad (1)$$

$$2\,H_2O + 4\,h^+ \rightarrow O_2 + 4\,H^+ \qquad \text{Oxidation half reaction} \qquad (2)$$

$$2\,H_2O + 2\,O_2 \rightarrow 2\,H_2 \qquad \text{Overall water splitting} \qquad (3)$$

Konstantinos Christoforidis obtained his PhD from the University of Ioannina (Greece) working on the development and application of biomimetic catalytic systems. Since then he focused on the development of photoactivated nanomaterials applied in environmental depollution and sustainable energy production. He is currently working on the synthesis of advanced multifunctional materials for solar fuels production.

Paolo Fornasiero obtained the Ph.D. in chemistry in 1997 at the University of Trieste (Italy). After a postdoctoral fellowship at the University of Reading (UK), he was appointed as an assistant professor in 1998, associate professor in 2006 and full professor of inorganic chemistry in 2016 at the University of Trieste. He received the Nasini Gold medal in 2005 for his contribution in Inorganic Chemistry and the Chiusoli Gold medal in 2013 for his studies in catalysis by the Italian Chemical Society. In 2016, he received the Heinz Heinemann Award for his contribution to catalyst science and technology from the International Association of Catalysis Societies.

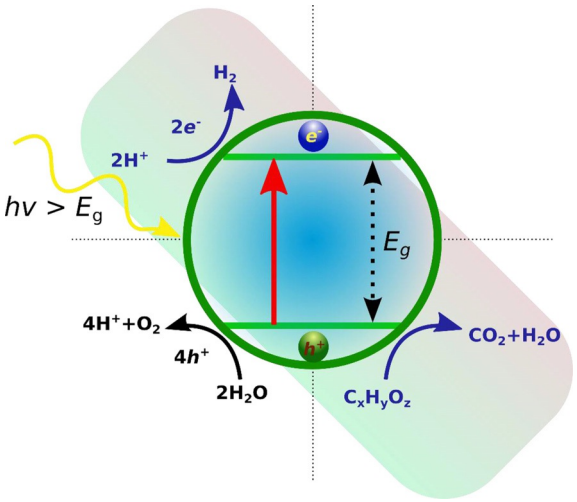

Figure 1. Schematic representation of redox reactions that take place on a photocatalyst after e^-/h^+ pairs are generated under light irradiation with energy higher than the E_g of the semiconductor. Water splitting (left-hand reactions) and oxygenates ($C_xH_yO_z$) oxidation under anaerobic conditions. The rectangular highlights the photoreforming process.

$$C_xH_yO_z + (2x-z)H_2O \rightarrow (2x-z+y/2)H_2 + x\,CO_2 \qquad \text{Photoreforming} \qquad (4)$$

The importance of photocatalysis in H_2 production has been expressed by the fast growth of literature reports including reviews. The WS reaction has been reviewed extensively[8] while the photoreforming process is less documented.[7,9] The present Review is a comprehensive, systematic, and up-to-date review, outlining the effect of the sacrificial agent and the co-catalyst used, presenting the advantages on the field in terms of novel photoactive materials and discussing the rationalization of the key parameters controlling activity. A brief introduction on the elementary steps of photocatalytic reactions will be given. The photoreforming process using oxygenates, carbohydrates and wastes, will be reviewed since pure WS or the use of sacrificial agents simple for charge consumption are more straightforward processes. The effect of using different organic substances on H_2 production will be critically discussed. Considering that recent developments in novel synthesis strategies allowed discriminating the effect of key materials properties on activity, herein the crucial effect of the cocatalyst will be critically analyzed. Finally, the recent progress related with the photocatalyst development will be discussed with particular attention to novel organic and hybrid organic/inorganic photocatalysts.

2. Photocatalytic Principals and Drawbacks—Elementary Steps

A chain of events must take place in order to guarantee the occurrence of a photocatalytic reaction in the presence of a semiconductor (SC). These are summarized in Figure 1 for both pure WS and photoreforming process under anaerobic conditions. The first and most crucial step is light absorption

and the formation of charge carriers (electron and hole pairs, e^-/h^+). Preferentially e^- and h^+ formation should take place under solar light irradiation making use of the visible region of light. When a SC is exposed to light irradiation of energy higher than its band gap energy (E_g), e^- from the valence band (VB) are excited to the conduction band (CB) leaving behind h^+. The photogenerated e^- and h^+ can follow several paths. Bulk and surface recombination can occur releasing heat, hindering activity. Once separated and transferred on the surface of the catalyst, these e^-/h^+ pairs are able to perform reduction and oxidation reactions.

The realization of a specific reaction is strictly related to the

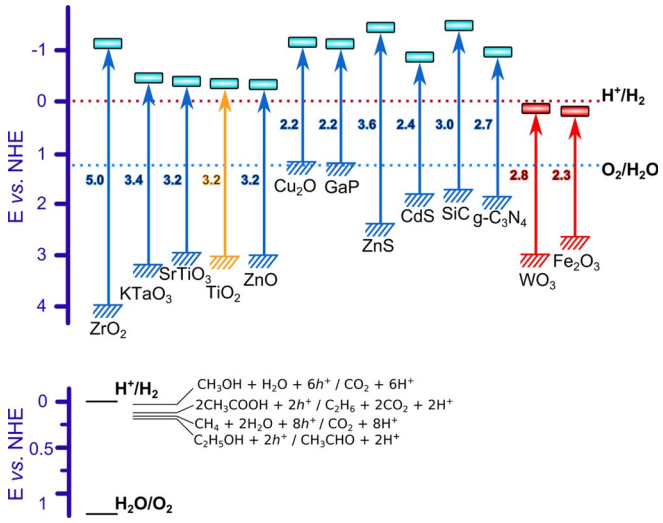

Figure 2. Upper panel: Band gap energies and band position of several semiconductors in relation with the redox potentials of WS. The position of the CB and VB edges are presented relative to the NHE at pH 0. Lower panel: Oxidation potentials of several organics and their position with respect to redox potentials of WS.

actual band structure of a SC (Figure 2). The CB and VB edge potentials define the reduction and oxidation ability of e^- and h^+, respectively. In the case of H_2 photoproduction, the bottom of the CB must be more negative than the H^+/H_2 redox couple (0 V vs. NHE, pH 0). In the WS process, in order for the oxidation half reaction to occur the top of the VB should be more positive than the oxidation potential of O_2/H_2O (1.23 V vs. NHE, pH 0). Therefore, the theoretical minimal E_g for WS is 1.23 V. In practice this value rises to 2.0–2.4 eV, owing to kinetic overpotentials and energy losses during the process. In terms of thermodynamics, the WS reaction is an uphill reaction as evidenced by the large positive charge in Gibbs free energy ($\Delta G^0 = +237.2\ kJ\,mol^{-1}$). This is attributed to the endothermic oxidation half reaction, which is however essential for the overall process providing protons and e^- for the reduction half reaction. The highly demanding oxygen evolution reaction is the bottleneck of the pure WS reaction since there are few narrow E_g materials that can catalyze both half reactions. Notably, working at neutral pH or pH > 0 is thermodynamically more challenging due to the lower proton availability.

Usually, to evaluate the activity of photocatalysts, sacrificial agents are used to monitor the efficiency towards one of the two half reactions. However, active materials for one of the two half reactions in the presence of a sacrificial agent are not necessarily active for the overall WS process. In contrast to the pure WS, organic substrates used in the photoreforming process present lower oxidation potentials (0.08 V vs. NHE for ethanol)[10] (see Figure 2) scavenging h^+ more efficiently and therefore consuming faster h^+ preventing charge recombination, while, at the same time they can serve as proton source.[11] Therefore, from a thermodynamic point of view the photoreforming process is less demanding process compared with the pure WS reaction[12] and diminishes in parallel the H_2 and O_2 backward reaction.[13] For such a process to be considered realistic, the sacrificial agents used must be abundant and continuously available, produced without competing for land used for food production, and of low cost if not renewable. In principle, various bioavailable substances can serve this role.

Different SC have been developed and applied in photoassisted H_2 production reactions. Despite the huge efforts and the promising results, efficiency is still far from practical applications. Among the different photocatalysts applied TiO_2 is the most studied, owing to its inherent properties (non-toxic nature, cheap, high chemical stability). However, TiO_2 exhibits relatively fast recombination rates and is a wide band-gap semiconductor ($\approx$3.2 eV for anatase) absorbing light in the near UV region.[14] This diminishes the efficiency under sun light since UV accounts for only 3–4% of the solar energy. It is generally accepted that an efficient photosystem must possess 1) efficient solar light harvesting and generation of redox equivalents, 2) stability under working conditions and 3) be cost-effective. The main technical challenges in the design of suitable semiconductors include achieving 1) effective charge-carrier separation, 2) fast diffusion of the photoproduced e^- and h^+ and 3) their migration to surface reactive centers, 4) correctly alignment of the band edges with the redox potentials of the desired reactions, 5) exposed active centers and 6) simple material synthesis avoiding the use of rare materials. It is clear, therefore, that efficiency depends primarily on material engineering, which should aim at improving the key parameters mentioned.

3. Using Oxygenates for H_2 Production—Photoreforming Process

H_2 photoproduction from water and various organic compounds in the presence of a SC was first demonstrated in the early 80's. A variety of organic compounds was used, including methanol,[15] ethanol,[16] sugar,[17] amino acids and proteins, raw biomass,[18] aliphatic/aromatic compounds, fossil fuels,[19] CO,[20] ethylene,[21] and lactic acid[22] over TiO_2 and CdS catalysts. Compared with pure WS, the increase in the observed H_2 production was attributed to the lower Gibbs free energy change and the production of CO_2 as the product of the oxidation half reaction instead of O_2.

Since these early reports, the field of photocatalytic H_2 production from water using carbon containing compounds as

sacrificial agents has gained significant attention.[9] Research has mainly focused on the improvement of the catalysts properties, but also on mechanistic aspects and how the nature of the sacrificial agent affects efficiency. Different organic compounds have been investigated. Among them methanol is employed most often, owing mainly to its structure simplicity that helps understanding reaction mechanism, its high H-content and its potential to capture h^+. Ethanol is also widely studied, as it is only slightly more complex than methanol, having only one C–C bond difficult to activate, but at variance with methanol, it is not toxic. Bio-available compounds such as ethanol, glycerol, and sugars originating from biological substrates or even wastes are particularly attractive for the photoreforming process.[9] In the following section, we will present some of the most used organic sacrificial agents in photoreforming process for H_2 production.

3.1. Sacrificial agent: Methanol

Methanol, as the simplest alcohol, containing only one hydroxyl group and one carbon atom, is considered the model molecule for the photocatalytic H_2 production reaction. Consistently, it was the ideal feedstock for the early studies on the photoreforming mechanism. H_2 production by methanol photoreforming was reported in 1980 by Kawai and Sakata[15] who proposed a reaction mechanism that proceed through the initial formation of formaldehyde, followed by its oxidation to formic acid as intermediates and finally its decomposition to CO_2 and H_2. A systematic study was done by Chiarello et al. using TiO_2 functionalized with a series of noble metals (Ag, Au, Pt).[23] A correlation between activity and the work function values of the cocatalyst was observed.[23,24]

In situ studies performed at ambient or near ambient temperatures using metalized TiO_2 suggested the stepwise oxidation of methanol on the surface of TiO_2 by photogenerated h^+ releasing protons and forming HCOH and eventually HCOOH.[25] The oxidation steps have been also suggested to proceed via an indirect path involving $OH^\bullet$ attack.[26] Whereas the methanol photoreforming process proceeds from the VB h^+ (either direct or indirect), H_2 evolution takes place on the cocatalyst.[24,25,27] It has been suggested that H^+ originating from both H_2O and methanol is used to generate H_2 in methanol photoreforming,[25a] and that increasing the methanol concentration significantly increases H_2 photoproduction.[28] The sorption of methanol, as well as the catalytic profile regarding by-products formation, depends greatly on the conditions used, such as the water/methanol ratio.[23,29] However, HCOH and HCOOH are considered the dominant oxidation intermediates.[23–,25c,30] The suggested overall reaction over TiO_2 under irradiation is the following [Eq. (5)–(7)]:[30b,31]

$$CH_3OH \rightarrow HCOC + H_2 \quad (5)$$

$$HCOH + H_2O \rightarrow HCOOH + H_2 \quad (6)$$

$$HCOOH \rightarrow CO_2 + H_2 \quad (7)$$

The catalytic conditions may also affect activity. Bahruji et al. reported that H_2 production over a Pd/rutile TiO_2 catalyst is 10 times higher when the reaction is performed in the gas phase compared with the liquid phase.[32] They suggested that the improved gas phase activity is related with the higher relative concentration of methanol and the reduced competition with water for adsorption.

3.2. Sacrificial agent: Ethanol

Ethanol has been widely investigated as sacrificial agent for the production of H_2 mainly because it can be produced on a large scale from renewable biomass, including from cellulose or lingo-cellulose.[6] Ethanol photoreforming involves the formation of acetaldehyde and acetic acid as in the following [Eq. (8)–(9)]:

$$C_2H_5OH + 2\,h^+ \rightarrow CH_3CHO + 2\,H^+ \quad (8)$$

$$CH_3CHO + H_2O + 2\,h^+ \rightarrow CH_3COOH + 2\,H^+ \quad (9)$$

with the concomitant production of H_2 via H^+ reduction.[16,33] Acetic acid and acetaldehyde may undergo further oxidation in parallel.[16] In addition to the direct reaction of ethanol with h^+, formation of acetaldehyde was also proposed to be initiated by the spontaneous formation of ethoxide on the surface of TiO_2 followed by h^+ oxidation,[34] or via ethanol oxidation by $OH^\bullet$.[35] Acetaldehyde has always been found as the main by-product, however, other products such as CH_4, CO_2, CO, C_2H_4, C_2H_6, have been also detected in various ratios.[36] Based on the CO_2 and H_2 produced, complete ethanol photoreforming has been reported over Pt/TiO_2 catalysts, presenting 50% apparent quantum yield (QY) of H_2 evolution at 365 nm.[37] Recently a 65% QY for H_2 production was reported using 1D brookite nanorods.[38] Acetaldehyde and 1,1-diethoxyetane were produced via dehydrogenation while no CO_2 was observed suggesting that ethanol oxidation takes place more readily than acetaldehyde.

3.3. Sacrificial agent: Glucose

H_2 production from saccharides such as glucose reforming is thermodynamically a favorable reaction since the change of Gibbs free energy gives a negative value.[39] Glucose can be obtained from the hydrolysis of cellulose. High content of sugars is also found in wastewaters from food processes. Therefore, many catalysts have been tested for H_2 photoproduction using glucose as model for biomass.[12,37,40] In 1983 John et al. first studied the mechanism of glucose photoreforming over a Pt/TiO_2 catalyst.[41] They proposed that the –OH and –CHO terminal groups are oxides by photogenerated h^+, liberating protons and producing –COOH groups which undergo decarboxylation with CO_2 evolution [Eq. (10)–(12)]:

$$R{-}CHO + H_2O + 2\,h^+ \rightarrow R{-}COOH + 2\,H^+ \quad (10)$$

$$R{-}CH_2OH + H_2O + 4\,h^+ \rightarrow R{-}COOH + 4\,H^+ \quad (11)$$

$$R{-}COOH \rightarrow RH + CO_2 \quad (12)$$

H_2 production takes place on the platinized surface via conventional reduction from the photogenerated e^-. The reaction of glucose with $OH^\bullet$ has been also proposed for the production of gluconic acid that is further oxidized to CO_2.[40b,d] Zhou et al. studied the effect of D-glucose epimerization on H_2 production over a Pt loaded TiO_2 catalyst.[42] They suggested that the lower catalytic activity when using the β-D-glucose as sacrificial agent originates from its lower adsorption on the surface of TiO_2. This underlined the importance to modulate the interaction between the photocatalyst and the sacrificial agent to bust the activity. In general, the presence of functionalities, i.e. –OH or C=C, favors the adsorption on the surface. Enhanced adsorption is directly translated to a quick diffusion of the sacrificial agent on the surface of the catalyst and an effective scavenging of h^+ species, providing in parallel readily available H^+. A detailed reaction mechanism of glucose photoreforming process was proposed by Fu et al.[43] The mechanism includes the bonding of glucose with undercoordinated surface Ti-sites through hydroxyl oxygen atoms, dissociation of H^+, subsequent oxidation and decarboxylation reactions resulting eventual in CO_2 production (Figure 3). Improvement of H_2 production via glucose photoreforming has been achieved by optimizing the catalyst properties. Studies focused on improving the textural properties of the catalyst, enhancing glucose adsorption, but also controlling the strength of the cocatalyst/semiconductor interaction and the actual band structure regulating charge migration.[12,40b–d,f,g] In addition to glucose, Caravaca et al. recently demonstrated that H_2 may be efficiently produced directly from the photocatalytic reforming of cellulose using noble-metal and Ni loaded TiO_2.[44] The authors suggested that hydrolysis of cellulose into glucose is the first step in the photoreforming process.

3.4. Sacrificial agent: Glycerol

The use of glycerol as sacrificial agent for H_2 production via the photoreforming process is particularly interesting. Glycerol is produced in large amounts being a 10 wt% by-product of the biodiesel industry while it has still a limited demand in the market. Therefore it is considered as waste and its use in H_2 production, serving both as H-source and e^- donor, may reduce additional disposal costs.[11,45] Various catalysts have been tested, the most investigate of which are again TiO_2 based nanostructures.[46] Although different intermediate products have been detected depending mainly on the catalyst used,[36a,45b,47] the same main reaction products have been observed in most studies either in the liquid phase photoreforming or even the gas phase steam reforming of glycerol including the formation of ketones, alcohols, and acids.[36a,48] Montini et al. using Cu/TiO_2 nanocomposites under simulated solar light irradiation reported the presence of 1,3-dihydroxypropanone and hydroxyacetaldehyde as the main by-products in the liquid phase and CO_2 and H_2 in the gas phase.[36a] The full photoreforming of glycerol to H_2 and CO_2 proceeds through the formation of 2,3-dihydroxypropanal and the subsequent formation of alcohols, aldehydes, and carboxylic acids. The initial steps of glycerol oxidation have been proposed via the chemiadsorption of glycerol, the direct oxidation by h^+ resulting in the breaking of C–H bond and the formation of a ketyl radical that transfers the electron on TiO_2 followed by release of the keton.[46a]

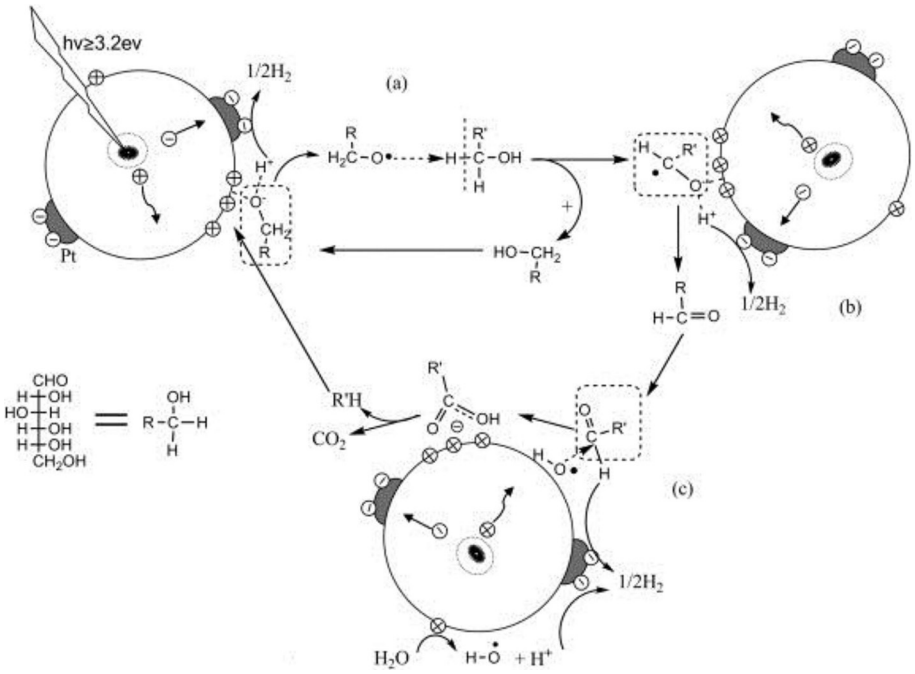

Figure 3. Proposed mechanism of the photocatalytic reforming of glucose on Pt/TiO_2. Reprinted from Ref. [43] with permission from Elsevier.

Using a Pt/TiO_2 catalyst dispersed in aqueous solutions under simulated solar light Kondarides and co-workers observed only CO_2 and H_2 in the gas phase, whereas many of the products were in the liquid phase,[45b,47a,48a] originating from both the oxidation and reforming process.[48a] The experimentally observed CO_2 and H_2 amounts were in excellent agreement with the theoretically predicted stoichiometry, suggesting complete reforming of glycerol to CO_2 and H_2.[37,45b,47a] The efficiency of light-to-chemical energy conversion increased with increasing glycerol concentration and high values were obtained (31%) under UV light irradiation attributed to the suppressed H_2/O_2 back reaction.[37] Bowker and co-workers suggested that H_2 evolution on Pd/TiO_2 proceeds through the dissociation of adsorbed glycerol molecules with the concomitant production of CO.[50] In this scheme, photoactivated oxygen species formed on the oxide migrate to the Pd and react with CO removing it as CO_2.

3.5. Sacrificial agent: Pollutants and wastes

The use of organic pollutants present in water or wastewater as sacrificial agents is definitely an attractive process with a dual role: wastewater treatment with the simultaneous production of H_2. H_2 production over Pt/TiO_2 was evidenced using benzene and phenol as e^- donors.[19] The authors proposed a direct oxidation of benzene by photogenerated h^+, the formation of phenol and catechol followed by ring opening and finally CO_2 production. Photoreforming of phenol over platinized TiO_2 nanotubes presented 12 times higher H_2 production rate compared with the pure WS process.[46a] Choi and co-workers studied the degradation of 4-chlorophenol, bisphenol A, urea and urine under anoxic condition and the concurrent production of H_2 over fluoride or phosphate modified TiO_2 with different metal cocatalysts.[49,51] They attributed the enhanced activity to a synergistic effect of the anions and the metals deposited on the TiO_2 surface that increases the interfacial charge transfer. Surface fluorides and phosphates affect the adsorption of organic substrates, eliminating external charge recombination centers (Figure 4).

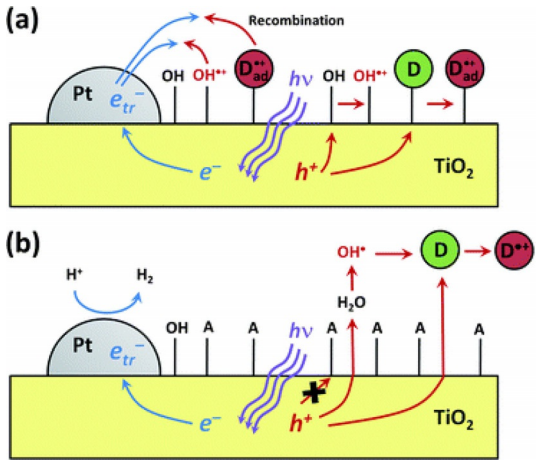

Figure 4. Schematic illustration of the interfacial charge transfer and recombination occurring on a) Pt/TiO_2 and b) F-TiO_2/Pt (or P-TiO_2/ Pt). A represents the surface adsorbed fluorides or phosphates and D indicates the organic substrates. Reproduced from Ref. [49] with permission from The Royal Society of Chemistry.

Patsoura et al. studied the production of H_2 and the simultaneous mineralization of common pollutants (alcohols, organic acids, aldehyde) originating from biomass processing industries over a Pt/TIO_2 catalyst under simulated solar and UV light irradiation.[13] The H_2 production rates were correlated with the photodegradation rates of the organic compounds used and their size-dependent mobility. Li and co-workers studied the effect on H_2 production of different pollutants in single component or mixed systems over a Pt/TiO_2 catalyst.[52] Using oxalic acid, formic acid and formaldehyde as sacrificial agents they showed that H_2 production is linked with the adsorption affinity of these compounds on the surface of the catalyst determined using in situ IR spectroscopy.[52a] They also demonstrate that inorganic anions, commonly found in industrial wastes presenting high affinity to adsorb on the surface of the catalyst, hinder H_2 production via competitive inhibition for adsorption with the sacrificial agent.[52b] H_2 production and simultaneous dyes degradation has been also shown to proceed over TiO_2 based photocatalysts.[53] Here again, the dyes enhance charge separation acting as scavengers of photogenerated oxidizing agents while enhanced adsorption of the dye on the catalyst increased H_2 production. In a more appealing application of the process, H_2 production over titania-based catalysts was demonstrated using wastes as feed-stock. Liu et al. studied the degradation of waste activated sludge and the simultaneous production of H_2 using Ag/TiO_2.[54] Photocatalytic H_2 production under UV and simulated solar light irradiation was also demonstrated using olive mill wastewater as feed-stock.[55] The catalytic conditions related with the key parameters of the catalytic process (substrate concentration, pH value of the reaction mixture, amount of the catalyst used and irradiation time) were optimized. In parallel to H_2 production, an optimum of 84% degradation of the waste was achieved using light irradiation in the range 100 to 280 nm[54] while no significant degradation was observed at longer wavelengths (366 nm).[54]

4. Photocatalytic Reactivity

Undoubtedly, the physical and electronic characteristics of the catalyst determine photoactivity. Recent theoretical contributions suggest that efficiency is governed by recombination processes in the bulk of the catalyst that affect the number of photogenerated charges reaching active sites.[56] Many technical factors have been also found to affect the photocatalytic H_2 production. These includes the pH value of the reaction mixture, the temperature as well as the phase (liquid or gas-stream) where the reaction is performed, the concentration of the sacrificial agent used and the amount of the catalyst in the suspension. To add to the complexity of the system, some of the above mentioned factors depend greatly on the SC used. For example, the amount of the catalyst where the optimal reaction rates can be achieved may vary significantly from sample to sample, depending on the absorption coefficient,

photon scattering/reflection and the catalyst degree of suspension.[57] These issues caused inconsistencies in reporting activity and made difficult the comparison of catalytic systems reported in the literature.[58] The technical parries have been recently outlined by Qureshi and Takanabe.[58]

A critical parameter that must be taken always into account is the stability of the catalyst. For practical applications, a photocatalyst must not only be highly efficient in H_2 production but also stable. Stability tests can be done by performing long-time catalytic reactions or repeated experiment. To establish the stability against photocorrosion phenomena, thorough characterization of the catalyst must be performed after the catalytic tests. An indicator of the catalyst stability is the constant increase of the products concentration or stable reaction rates (steady state) under extended irradiation period in batch and contentious flow reactor set-ups, respectively. Stability is a common problem for metal sulfides and dye-sensitized SC using either metal complexes or organic sensitizers. Attempts have been performed in both cases to solve this problem via chemical fixation of dye molecules,[59] encapsulation, the development of core–shell materials and protecting surface layers,[60] formation of composites that allowed facile charge carriers separation[61] or the use of specific sacrificial agents as h^+ scavengers such as S^{2-} and SO_3^{2-} in the case of sulfides to suppress photocorrosion.[62]

Nevertheless, among the different factors that affect activity, of particular importance is the nature of the sacrificial agent and the cocatalyst used. These two parameters are discussed in the following.

4.1. Different sacrificial agents

As a general role, the presence of hydroxyl groups in the sacrificial agent is considered essential for efficient H_2 evolution.[50,63] In addition, in most studies the increase of the structure complexity of the sacrificial agent used resulted to decreased H_2 production rates,[40a,64] although some controversial results have been also reported in the literature. Using C3-polyols (glycerol, propyleneglycol, and isopropanol) Fu et al. reported that increase of the OH-groups in the structure of the sacrificial agent results in increased H_2 and CO_2 evolution over a Pt/TiO_2 catalyst.[46a] This was attributed on the dual function of the OH-groups: 1) providing an anchor for the chemical absorption on TiO_2 and 2) serving as an effective h^+ scavenger.

The catalytic H_2 production rates over a Pt/TiO_2 catalyst using the same concentration of different alcohols (5 vol.%) increased in the following order: ethanol > isopropanol > *n*-butanol > methanol.[28] However, at higher alcohol percentage the performances in the presence of ethanol and methanol were more comparable. In most of the studies, the use of methanol as sacrificial agent compared with other alcohols resulted in enhanced H_2 production rates.[60b,65] This is attributed to the fast h^+ transfer process.[66] H_2 production rates have been found higher using primary compared with secondary alcohols over Au/TiO_2 catalysts while the catalytic activity was much smaller using tertiary alcohols.[67] The polarity of the alcohol used, which essentially affects the dissociative adsorption on the TiO_2 catalyst, has been considered as one of the parameters that controls H_2 production at least for mono-hydric alcohols, although the acidity and the steric hindrance may also affect activity.[34a,46b,64c,68] The kinetics of electron transfer reactions between alcohols (e.g. e^- donors) and VB h^+ (a factor linked with the oxidation potential of the sacrificial agent) has been also shown to affect H_2 evolution over titania-based catalysts.[66] Based on studies using various alcohols it has been shown that an essential parameter for H_2 production via the photoreforming process is the presence of α-hydrogens on the carbon where the OH-group is attached.[64b,69]

In an effort to get insights into the photocatalytic mechanism using different sacrificial agents, the effect of the oxidation products of the parent sacrificial agent was studied. In the case of methanol, higher H_2 production rates were achieved using formic acid or formaldehyde over different photocatalyst.[60b,65,71] On the contrary, lower rates were achieved using acetaldehyde and acetic acid compared with ethanol over Pt/TiO_2 catalyst.[64b,69b] This means that the intermediate products formed using different sacrificial agents may have an opponent effect on photoactivity. In addition, H_2 production rates depend greatly on the concentration of the sacrificial agent and concentration may differ significantly based on the sacrificial agents used.

4.2. Role of the Cocatalyst

Materials without the presence of a cocatalyst are practically inactive in H_2 evolution. Traditionally, noble metal nanoparticles have been used as cocatalysts. It is generally accepted that the cocatalyst can provide additional reaction sites and favors charge migration and separation. The reason behind this latter promotional effect relates with the formation of a Schottky barrier originating from the difference in the Fermi levels between the metal nanoparticles and the SC. This allows the injection of photogenerated e^- from the CB of the SC into the metal.[72] In addition, Bowker and co-workers suggested also a direct involvement of the cocatalyst in the reaction mechanism, participating in the initial steps of the reaction such as dehydrogenation/ decarbonylation of the sacrificial agent.[73] Recently, Joo et al. proposed that the cocatalyst can act as recombination center of "reduced H-atoms".[70] Using Au/TiO_2 as a model catalyst, they proposed a mechanism where protons are reduced on the surface of the SC, the obtained H^+ migrate to the metal cocatalyst and they recombine forming H_2 (Figure 5B). This was accomplished by employing model reactions using bare TiO_2 in the presence of reducible ions in the reaction mixture and monitoring O_2 evolution or using electron traps other than noble metal nanoparticles and monitoring H_2 evolution.

Many factors can affect the performance of the cocatalyst. Normally, there is an optimum cocatalyst amount towards enhanced photoactivity which varies depending on the cocatalyst used. Initially, catalytic activity increases with increasing cocatalyst loading on the surface of the SC. At a certain point, further increase of the cocatalyst loading will result to decreased photocatalytic activity. This can be attributed to: 1) shading effects

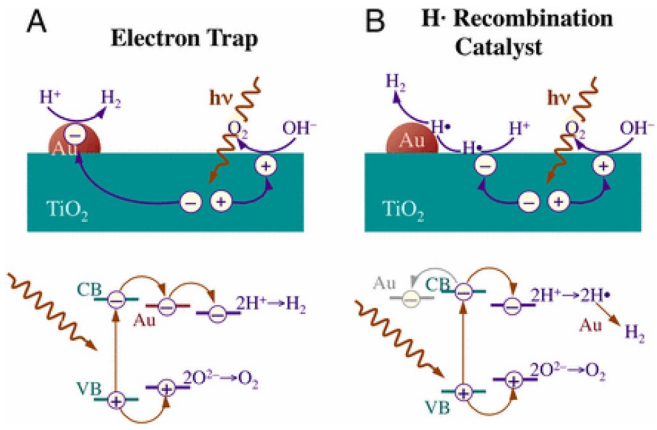

Figure 5. Schematic representation of the mechanisms (Upper) and electronic transitions (Lower) proposed to explain the role of metals (Au) in the photocatalytic splitting of water with SCs (TiO_2). A) The metal acts as an e^- trap that physically separates the excited e^- used for proton reduction from the oxidation step that occurs on the surface of the SC. B) H^+ reduction occurs at SC sites but that the resulting hydrogen atoms need to migrate to the metal to recombine and produce the final H_2 product. Reproduced from Ref. [70].

caused by excess cocatalyst loading; 2) increase of the particle size with increasing cocatalyst's content, with detrimental effects in charge recombination and specific surface area. The Fermi level equilibrium may also be affected by the size of the metal nanoparticle;[74] 3) shielding effects by covering active sites of the catalyst for oxidation or reduction reactions and, 4) reduced cocatalyst dispersion on the surface of the SC.

Pt appears to be one of the best candidates as cocatalyst, owing to its large work function.[75] Fu et al. studied the H_2 production rate from the photocatalytic reforming of glucose over different noble metal loaded TiO_2 photocatalyst.[43] The specific activity was in the following order: $Pt/TiO_2 > Au/TiO_2 > Pd/TiO_2 > Rh/TiO_2 > Ag/TiO_2 > Ru/TiO_2$. The enhancement of the photoactivity in the presence of the cocatalysts was attributed to the formation of Schottky barrier while the observed trend to the difference of the work functions of the metals: metals with larger work function resulted in stronger Schottky barrier effect, enhancing charge separation and improving activity. Similar trends have been reported for the methanol photoreforming process.[23,76] Exceptions on the above rule have been observed in the case of Au and Pd which seems more complex. For example, H_2 production rates decreased in the order $Pd/TiO_2 > Pt/TiO_2 \approx Au/TiO_2$ using different sacrificial agents.[66] This was attributed to a combination of different factors including the higher density of states in the vicinity of the Fermi level of the Pd compared with that of Pt and Au and the lower electron affinity of Pd enabling an easier electron transfer from Pd to donor species. Recently, a detailed study from Jiang et al. revealed key parameters that control H_2 evolution in Pt/TiO_2 catalysts.[77] Using different deposition processes for the development of Pt nanoparticles on TiO_2, they concluded that the photodeposition process is superior because it allows the selective deposition of Pt on suitable e^- trapping sites that shorten the transferring pathway of e^- from the bulk to the surface. In addition, internal-to-external reduction process permits the total reduction of Pt and its intimate deposition on the oxide. However, detailed sorption studies suggested that Pt deposition is facet-specific in platelike WO_3 crystals, determined primarily by differences in intrinsic surface charge rather than the preferential migration and collection sites of photogenerated charges.[78] These examples indicate that the deposition of the same cocatalyst on different photocatalysts may vary significantly.

The particle size of the cocatalyst is another critical parameter.[77,79] This was clearly demonstrated by Shen et al. using Au/CdS photocatalysts. Photoactivity was 11 times higher when sub-nm Au nanoparticles were used as cocatalysts compared with 9 nm Au.[80] Increasing the size of the Au cocatalyst higher than 12 nm also resulted in decreased H_2 production rates over Au/TiO_2 catalysts.[79]

Bowker et al. studied the photocatalytic production of H_2 over Pd and Au loaded TiO_2.[67] Pd showed superior activity compared with Au catalysts. This difference was attributed to 1) the electron affinity of the cocatalyst and 2) the actual mechanism of the photoreforming process over the Pd and Au cocatalysts. Since the electron affinity of Au is higher than that of Pd, e^- are trapped more efficiently by Au, which may affect the stability of surface intermediates and the e^-/h^+ recombination rate. The adsorption as well as the stability of certain reaction intermediates on Au and Pd varies significantly with a concomitant effect in the overall H_2 production rate. In addition, photoactivity was also affected by the method applied for the deposition of the cocatalyst that controlled the detailed morphology and the interaction with the SC. More sophisticated shell-protected metal nanoparticles using 11-mercaptoundecanoic acid as shell have been also developed and applied in H_2 production. In this case, the thiol groups of the ligand interact with the metal nanoparticles offering protection against agglomeration and allowing a homogeneous dispersion of the cocatalyst.[83] Using methanol as sacrificial agent, $Rh(OH)_3$ and Rh_2O_3 over Nb-based catalysts were proven more active for H_2 evolution against the corresponding Pt loaded catalysts.[85]

In addition to the monometallic cocatalysts, recent studies have demonstrated that SCs functionalized with bimetallic cocatalysts present superior photoactivity against H_2 production. Different materials have been prepared and tested, including noble and non-noble metals, hetero- and homo-metallic cocatalysts made of two metal elements. Au/Pd bimetallic cocatalysts loaded on TiO_2 presented a significant improvement in H_2 evolution compared with the monometallic counterparts (Figure 6).[67,81] This was attributed to the higher trapping electron ability by using alloy metal nanoparticles, originating from the lower Fermi level. A similar explanation was given for Ag/Pt bimetallic cocatalysts on TiO_2, highlighting also the competition between Ag and Pt to gain electrons.[82] A schematic diagram including the Fermi levels and work functions for the mono- and bimetallic cocatalyst is illustrated in Figure 7.

The specific ratio of the two parts in a bimetallic cocatalyst as well as the amount of the bimetallic cocatalyst may also affect photoactivity.[36c,86] Cheng et al. have shown that the optimum Pt/Au molar ratio in the core–shell bimetallic cocatalyst is 2. Lower amount of Pt is not enough to cover the surface of

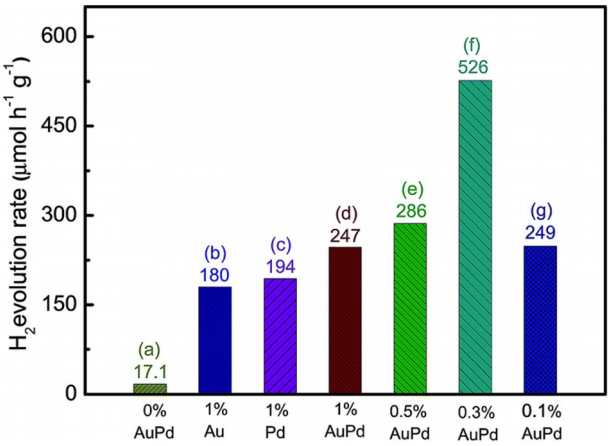

Figure 6. Rate of H_2 evolution over AuPd/TiO_2 composite samples with different AuPd contents, Pd/TiO_2 and Au/TiO_2 under UV-visible light. Reproduced from Ref. [81] with permission from The Royal Society of Chemistry.

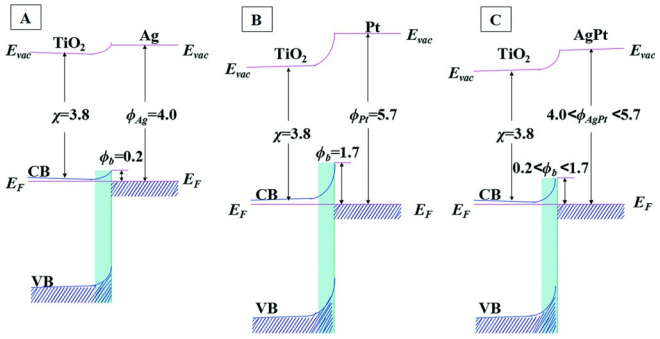

Figure 7. Schematic energy-band diagrams for A) Ag@TiO_2, B) Pt@TiO_2, and C) Ag/Pt@TiO_2 heterojunctions. E_{vac}, E_F, Φ_M, Φ_b, and χ denote vacuum level, Fermi level, work function of metal, Schottky barrier height, and electron affinity of the TiO_2 conduction band, respectively (in eV). Reproduced from Ref. [82] with permission from The Royal Society of Chemistry.

the Au core, while higher amount of Pt results also in the formation of isolated monometallic Pt nanoparticles.[81] A molar ratio in a comparable range was observed for Au/Pd core/shell bimetallic nanoparticles (25/75) immobilized on TiO_2.[86b] The improved activity of bimetallic cocatalysts was also evidenced in the photoreforming process of various renewable feedstock over Pt–Au/TiO_2, attributed to the alloy nature of the Pt/Au system.[36c]

Photoactivity presented also significant dependence on the preparation process such as the reduction process applied for the development of the monometallic and bimetallic cocatalyst. Materials prepared via reduction at 500 °C presented up to fourfold improvement compared with materials reduced at 250 °C.[36c] The structure/morphology of the bimetallic nanoparticle may also affect activity. Mizukoshi et al. demonstrated that Au/Pd core/shell nanoparticles on TiO_2 presented higher photocatalytic performance under visible light irradiation compared with random Au/Pd alloys of the same composition. Surprisingly, the trend was reversed under UV light irradiation.[86b] Au/Pd and Au/Pt core–shell nanostructures deposited on TiO_2 by chemical vapor impregnation method presented also higher H_2 evolution rates compared with the corresponding monometallic and Pd/Pt alloy cocatalysts.[87] Zhou et al. demonstrated that the structure of a ternary system made of CdS, Pd and TiO_2 affects H_2 evolution significantly.[84] CdS (core)/ Pd (shell) TiO_2 heterostructures (CdS/Pd/TiO_2) presented 4 times higher photoactivity compared with the corresponding material where the metal cocatalyst was deposited on the CdS/TiO_2 heterojunction (Pd/CdS/TiO_2) and 6.7 times than the bare CdS/TiO_2 binary heterojunction. This was attributed to the Z-

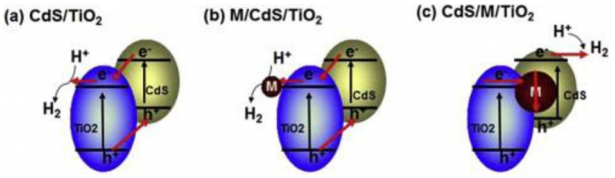

Figure 8. Schematic illustration of charge transfer in a) two-component and b) three-component and c) heterojunctions. Reprinted from Ref. [84] with permission from Elsevier.

Scheme like charge transfer mechanism in the CdS/Pd/TiO_2 case, enhancing charge separation and improving H_2 production from aqueous methanol solution (Figure 8c). Core-shell Au@TiO_2 structures decorated with CdS nanoparticles demonstrated high photocatalytic H_2 generation rates compared with the corresponding binary systems due to the unique CdS/Au@TiO_2 ternary structure, allowing the efficient transfer of photogenerated e^- from the CdS to the core Au particles while TiO_2 acted as the bridging part.[88]

Despite the high activity of noble metal based cocatalysts, in order to make H_2 generation a more energy-efficient and economical process, efficient noble-metal-free catalysts are required particularly in scale-up application. Therefore, of importance is to mention the progress over the last years on the development of cocatalysts based on non-precious metals employed in photocatalytic H_2 evolution reactions. Different transition-metal based cocatalysts have been prepared including oxides, hydroxides, sulfides. As in the case of noble metals, transition metal cocatalysts are believed to enhance charge separation and reduce the activation energy barrier for H_2 production.[89] Among the various earth abundant cocatalysts tested, Cu-based catalysts have been proven particular attractive,[90] however the performance is still lower compared with the noble metal cocatalysts. Recently, Bahruji et al. studied the H_2 production rate via methanol photoreforming using Cu, Ni, and Fe oxides loaded on TiO_2.[76b] The actual band structure related with the CB and VB energy level of the cocatalyst with respect to the TiO_2 has a crucial effect in H_2 evolution, defining the charge transfer mechanism and the part for H_2 production (Figure 9). These authors reported that the metal reducibility is the factor that determines photoactivity. They demonstrated that H_2 production increases as the enthalpy of reduction of the metal oxide decreases. Materials with positive enthalpy of reduction are practically inactive for H_2 evolution. However, proper treatment of the photocatalysts may convert inactive

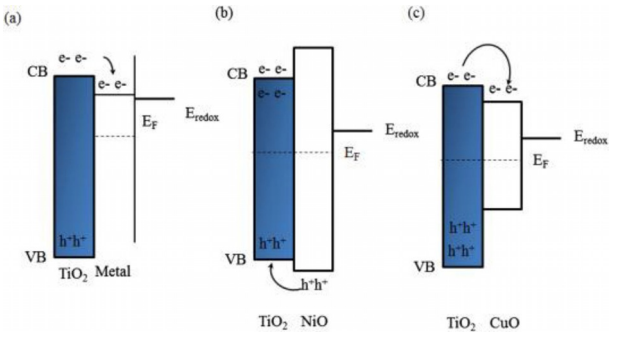

Figure 9. Energy levels of a) TiO_2/metal b) TiO_2/NiO, and c) TiO_2/CuO interfaces and charge transfer. Reprinted from Ref. [76b] with permission from Elsevier.

nanomaterials into efficient H_2 production catalysts.[76b] Simon et al. developed CuO/ZnO nanorod arrays and proposed that the 1D morphology and the p–n heterojunction results in enhanced e^-/h^+ pairs separation.[91] While the bare ZnO nanorods did not show any activity, the CuO/ZnO nanocomposites had appreciable performance. The H_2 production rates obtained by ethanol photoreforming depended greatly on the conditions employed in preparation process controlling the dispersion and the coverage of the ZnO part.[91] Embedded CuO_x/TiO_2 catalysts have been found more active for H_2 production via ethanol and glycerol photoreforming compared with materials prepared by classical wet impregnation methods.[92] The role of the SC as a support for Cu-based catalysts may also have significant effect in photocatalytic activity. H_2 production by methanol photoreforming over Cu/TiO_2 catalysts was investigated using titania nanoparticles prepared by different routes. It was found that the surface properties of the TiO_2 controls the Cu nanoparticles size and dispersion but also the oxidation of the sacrificial agent.[93] Ternary nanocomposite materials made of Cu, graphene and TiO_2 have been prepared and tested for H_2 production using methanol as sacrificial agent.[94] Owing to the synergetic effect between Cu nanoclusters and graphene, the Cu/graphene cocatalyst was proven highly efficient for H_2 production presenting comparable photoactivity with systems containing Pt as cocatalyst. Recently, TiO_2 catalysts containing low amount of Ni nanoparticles presented comparable photoactivity with noble metal loaded TiO_2 catalysts tested for glucose, cellulose[44] and ethanol photoreforming.[95] This was addressed to the high dispersion of Ni on the TiO_2. Ni-based catalysts (Ni and NiO) supported on graphene oxide sheets were tested for H_2 production from aqueous methanol solution.[96] The superior activity of the catalysts containing Ni nanoparticles was attributed to the more efficient charge separation. Metallic Ni nanoparticles encapsulated in carbon shell with high chemical and thermal stability were coupled with CdS and presented high H_2 production with an apparent quantum yield up to $\approx$20.5% under 420 nm.[60a] In addition, bimetallic Ni/Cu catalysts have been successfully incorporated on TiO_2, presenting longer electron lifetime, enhanced e^-/h^+ separation and easier charge transfer resulting in increased activity compared with the monometallic catalysts.[97]

Metal sulfides are also promising materials for H_2 photoproduction and have been frequently applied using different sacrificial agents. From this class of materials of importance is to mention MoS_2, non-toxic and relatively stable against photocorrosion phenomena compared with other metal sulfides.[98] Several studies have demonstrated that catalysts functionalized with MoS_2 present superior H_2 production with respect to their noble metal counterparts. MoS_2/CdS catalysts were proven more active than the corresponding noble metal-CdS catalysts under identical conditions using lactic acid as sacrificial agent.[99] The enhanced activity was attributed to the successful formation of a junction through the intimate contact between CdS and MoS_2, improving the charge separation. Similar results have been reported using different sacrificial agents including ethanol and glycerol.[100] CdS modified with metal-organic framework (MOF) and MoS_2 presented also higher H_2 production rates than the corresponding Pt-loaded catalysts (Figure 10).[101] Thin MoS_2 slabs have been successfully grown on carbon nitride forming a hybrid layered heterojunction.[102] These materials were proven stable under irradiation and presented enhanced H_2 production rates compared with the corresponding Pt-catalysts, attributed to the geometric similarities of the coupled materials. 2D nanojuctions made of TiO_2 nanosheets with exposed (0 0 1) facets and layered MoS_2 were also proven more active than the corresponding noble metal loaded catalysts for H_2 production from aqueous methanol solution.[103] The difference was attributed to the larger contact area between the 2D–2D structure of MoS_2 and TiO_2 sheets compared with the 0D–2D interaction of the Pt/TiO_2 composite leading to more efficient interfacial charge transfer (Figure 11). H_2 production from aqueous ethanol solution has been also reported using noble metal free ternary materials comprised of TiO_2, graphene and MoS_2 as cocatalyst.[104] Catalytic activity was linked with a synergetic effect between MoS_2 nanosheets and

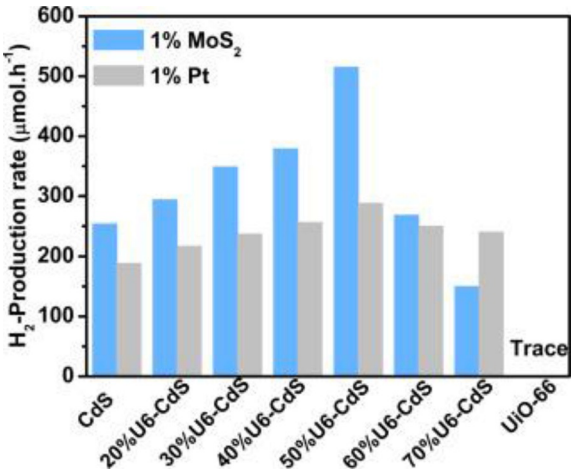

Figure 10. The rate of H_2 production over pure CdS, UiO-66 and U6-CdS composites loaded with 1 wt% MoS_2 or Pt. Reprinted from Ref. [101] with permission from Elsevier.

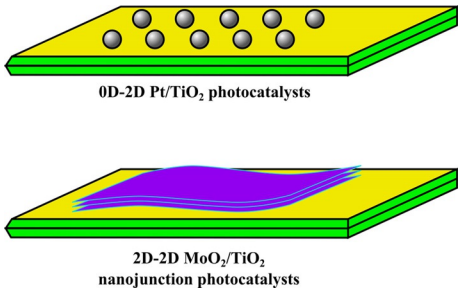

Figure 11. Schematic diagrams of 0D–2D Pt/TiO_2 and 2D–2D MoS_2/TiO_2 photocatalysts, demonstrating that the 2D–2D MoS_2/TiO_2 photocatalyst exhibits much larger contact interface between the light-harvesting SC and cocatalyst in comparison to the 0D–2D Pt/TiO_2 photocatalyst. Adopted from Ref. [103].

graphene, suppressing charge recombination, improving interfacial charge transfer and increasing the number of active adsorption sites and photocatalytic reaction centers. Photogenerated e^- from the CB of TiO_2 are injected into the graphene sheets while MoS_2 sheets act as e^- acceptors and active site for H_2 evolution.

Recently, metal phosphides (Ni_2P, Co_2P) have been employed as cocatalysts for H_2 production using CdS as a photosensitizer presenting significant activity under visible light irradiation.[105] Iron phosphide coupled with TiO_2 has been also shown efficient for photocatalytic H_2 production.[106]

It is clear therefore from the above examples that both the sacrificial agent and the cocatalyst used affect significantly the photocatalytic H_2 production. Concerning the sacrificial agent the results presented in the literature are relatively coherent. The sacrificial agent should: 1) contain OH-groups; 2) have simple structure; 3) have high affinity with the surface of the catalyst (polarity or the presence of groups acting as anchors); 4) have high electron donation ability. The presence of α-H atoms as well as the byproduct formation may also affect activity. In the case of the cocatalyst used, the field is not clear since different parameters may affect activity. However, charge separation seems to be the critical parameter that must be controlled. In general, the contact of the cocatalyst with the SC and the particle size must be tuned. Metal cocatalysts should possess large work function that will result in strong Schottky barrier effect, allowing efficient charge separation. However, future research should focus on the development of non-noble metal cocatalysts and the formation of heterojunctions. In this later case, the parameter that controls charge separation via interface is the difference in the CB energy levels of the two parts.

5. Photocatalysts for H_2 production

Suitable materials for photocatalytic H_2 production should primarily meet the fundamental electronic characteristics related with the band-edge energy positions (Figure 2). Many SCs have been prepared and tested. Among them, TiO_2-based photocatalysts occupy the vast majority of the reported photoactive materials.[38,39,107] However, despite the large number of studies using TiO_2, recent reports have shown that control of the structure at the nanoscale can still lead to significant improvement of photoactivity and demonstrated the potential for further investment in Ti-based materials.[38] Recently, Cargnello et al. using colloidal methods controlled the size of brookite nanorods manipulating the electronic properties related with charge transfer and separation, improving photoactivity.[38] Nevertheless, as in the case of most metal oxides, TiO_2 is a wide band-gap SC, a factor that diminishes the reaction efficiency under sun light. In this direction, recent studies have demonstrated the potential of black TiO_2 obtained by hydrogenation treatments in H_2 photoproduction. Since the proof-of-concept by Chen et al.,[108] different reaction conditions have been applied to prepare reduced TiO_2 with improved solar light absorption, charge transfer capability and photocatalytic activity.[109] Structural modifications induced during hydrogenation treatments include self-doped Ti^{3+} and oxygen vacancies, or incorporation of H-doping. The nature and location of defects as well as surface disorder are related with the charge separation efficiency and broad light absorption properties.[109c,110] Attempts are performed to explore more effective processes for the synthesis of reduced TiO_2, avoiding harsh reaction conditions.[111]

A number of strategies have been applied towards enhancing visible light absorption and improving charge separation. Traditionally, wide spectral response has been achieved by introducing impurities or incorporating sensitizers. Narrowing the band-gap energy has been accomplished via band gap engineering using dopants,[113] whereas organic dyes,[114] transition metal complexes,[115] or even narrow band-gap SCs[92,116] have been used as visible light sensitizers. Besides metal oxides, several metal chalcogenides possess suitable E_g and band-edge position for H_2 production under visible light irradiation.[60b,117] In terms of activity, CdS is an exceptional photocatalyst for H_2 evolution however is susceptible in photocorrosion phenomena with detrimental environmental impact, although improvements have been made in this aspect over the last years.[60a,61a,b] Plasmonic metal nanostructures have been also used to extent light absorption, imitating dye sensitization process. Three possible enhancement mechanisms have been proposed in plasmon photocatalysts: 1) enhanced light harvesting; 2) hot-electron injection, and 3) plasmon-induced resonance energy transfer.[118] The properties of plasmon photocatalysts are greatly affected by the nature but also the size of the particle. Plasmonic photocatalysts generally present efficient absorption in the visible region of light through localized surface plasmon resonance (LSPR) and low charge carrier recombination rate, owing to the nature of charge formation allowing fast migration of the carriers to the SC surface. The SPR induced charge formation close to the plasmonic nanoparticles permits e^-/h^+ pair formation near the surface of the material rather than in the balk. This allows efficient charge separation due to the surface potential, reducing in parallel their migration distance required to participate in redox reactions. Plasmonic metal nanostructures supported on insulating solids have been also found to catalyze photooxidation reactions of organic substrates.[119]

Pt nanoparticles have been also used as visible light absorbers. Different size Pt nanoparticles coupled with TiO_2[120] and other SC[121] allowed visible light driven oxidation reactions through direct charge transfer from Pt nanoparticles to TiO_2 CB. In these cases, visible light absorption was ascribed to SPR and intraband and interband transitions of Pt particles. The improvement of H_2 photoproduction under visible light irradiation using ternary Cu@CuO/g-C_3N_4/MCM-41 was also partially ascribed to SPR effect of Cu nanoparticles.[122] However, visible light activity of small Pd and Pt nanoparticles (1–6 nm) was ascribed to non-plasmonic effects.[123] Recently Zhang et al. established a new light absorption model to modulate the absorption peak of supported small Pt nanoparticles.[124] By selecting the proper support and fine tuning the synthesis method the authors observed localized absorption peaks originating from small Pt nanoparticles (< 10 nm) extending up to the visible region. This localized absorption can be tuned by adjusting the dielectric environment of the nanoparticles. Visible light activity was achieved using Pt/SiO_2 coated with a thin TiO_2 layer (Pt/SiO_2@TiO_2) while H_2 production increased with increasing Pt loading.

The presence of dopants, cocatalysts and the development of heterojunctions or homojunctions (inter-phase junctions)

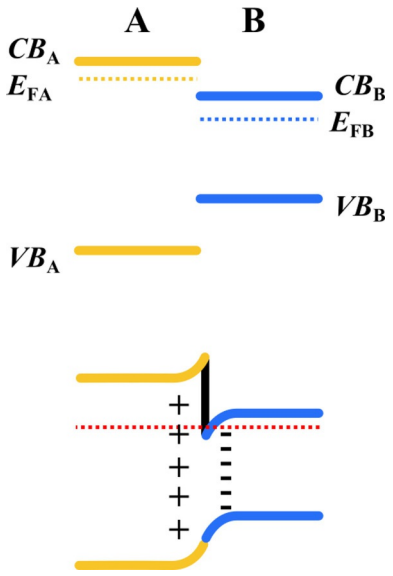

Figure 12. Energy band diagram of n–n type heterojunction in conduct (upper panel) and in equilibrium (lower panel) presenting the charge separation and the band bending at the heterojunction interface.

have been also shown to improve charge separation efficiency. In this later case, either one or both SCs are photoexcited and charge separation is driven by the difference in the band edge energy levels of the coupled SCs. Figure 12 presents the coupling of two n-type SCs (A and B) possessing different band and Fermi energy levels and the band bending at the heterojunction interface formed, owing to e^- flow from SC A (e.g. the one with higher Fermi energy level) to SC B. Depletion and accumulation regions are formed in SC A and B respectively, while at equilibrium the Fermi energy levels of both SCs are equal.[8d] This mechanism allows efficient charge separation, increasing the lifetime of the photogenerated charges and therefore activity.

In an analogous way, charge separation may also be achieved through the formation of a homojunction, even if the driving force of charge separation is smaller compared with

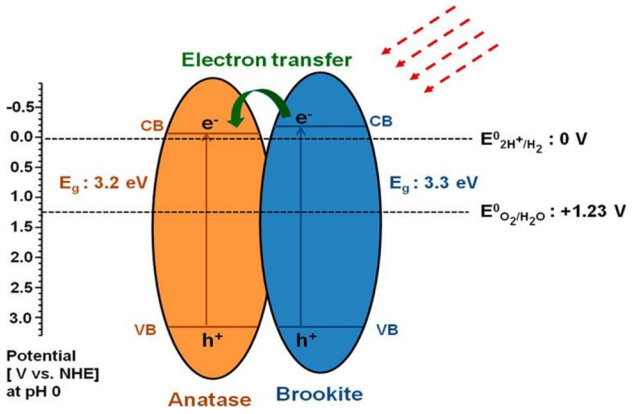

Figure 13. Charge separation in anatase-brookite TiO_2 homojunctions. Reprinted with permission from Ref. [112]. Copyright (2013) American Chemical Society.

the case of heterojunctions. Many such cases in the literature confirmed that inter-phase junctions, as for example in TiO_2-based catalysts,[36d, 112, 125] result in improved H_2 evolution through enhanced charge separation (Figure 13). Besides the more frequently observed charge separation due to differences in the band edge energy levels in heterojunctions, other charge transfer mechanisms have been also proposed. For example, in Type I core/shell CdS/ZnS nanocrystals, charge separation has been suggested to occur as a result of electron tunneling effect.[126] The potential differences of the Fermi energy level between reduction and oxidation cocatalysts and the band edges of the core CdS nanocrystal were suggested to play crucial role. In addition, Xie et al. suggested that charge separation takes place, owing to the presence of acceptor states within the band-gap in a similar core/shell CdS/ZnS system.[61b]

Of importance is to mention the advantages of the development of supported metal oxide nanostructures forming oxide layers. Different nanostructures including less explored metal oxides have been grown on suitable supports. Pure and coupled metal oxides such as different polymorphs of Fe_2O_3 (α-, ε-, β-Fe_2O_3),[40a, 127] VO_2,[128] Cu_2O and CuO,[129] Co_3O_4,[130] and CuO/ZnO[91] have been developed and tested for hydrogen evolution. Control of the composition and morphology at a nanometer scale controlled activity and allowed the development of active systems even in the absence of noble metal as cocatalyst. For example, H_2 production was greatly affected by regulating the CuO loading on the tips of vertically aligned ZnO nanorods (Figure 14).

Recently, the development of novel synthesis strategies allowed the development of more sophisticated nanostructured

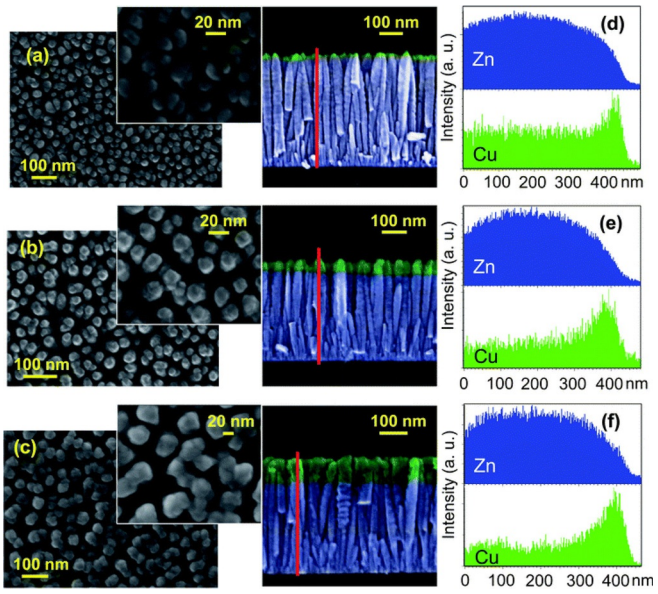

Figure 14. Plane-view/cross-sectional FE-SEM images (a–c) and EDXS line-scans (d–f) of CuO/ZnO specimens obtained at RF-power (radio frequency) values of 5 (a and d), 10 (b and e) and 15 W (c and f). EDXS line-scans were performed along the red line marked in the corresponding cross-sectional micrographs. The abscissa values increase from the deposit-substrate interface to the sample surface. In the FE-SEM cross-sectional views, the presence of CuO and ZnO are highlighted by green and blue colors, respectively, in accordance with EDXS line-scan analyses. Reproduced from Ref. [91].

materials and open-up new alternatives for the fabrication of advanced and more efficient catalysts, increasing the availability of nanomaterials for photocatalytic applications. Controlled synthesis processes allowed the development of nanostructured materials presenting unique properties compared to the corresponding bulk materials, catalysts of different morphology in the nanostructure (nanorods, nanowires, nanosheets) and the development of multiphase materials, nanocomposites and heterojunctions via the coupling of different SCs. In this regard, in addition to the well-studied metal oxides, special attention must be given on the recently developed pure organic and hybrid organic/inorganic catalysts making use of carbon-rich nanostructures. Recent developments in these types of nanomaterials include graphitic carbon nitride (CN, g-C_3N_4) based nanomaterials and the coupling of carbon nanostructures (CNSs) with inorganic nanomaterials for the development of nanohybrids. In many cases, the coupling of organic and inorganic materials revealed the concept of synergy between the two phases and the morphology at the nanoscale in improving photocatalytic performance.

5.1. Carbon nitride based nanomaterials

Over the last years, CN has emerged into a promising candidate for H_2 production driven by its 2D morphology, chemical stability under working conditions and visible light response. The polymeric nature of CN permits modification of its textural properties, morphology and electronic structure related with E_g, band-edges energy level, conductivity etc. The properties and synthetic strategies adopted for the developed of g-C_3N_4 based materials have been recently extensively reviewed.[132] In general, two approached have been used for the development of photoactive CN materials. The first is the bottom-up approach where nitrogen containing organic precursors are assembled usually through thermal polycondensation. The second, the top-down strategy, involves the post treatment of preformed g-C_3N_4. In the case of H_2 photocatalytic production, physical and chemical approaches have been adopted for improving the efficiency of CN based photocatalysts. It should be noted that even small changes in the synthesis process may result in significant change in photoactivity. For example, the use of different precursor or temperature affects the extent of polymerization and protonation, with a concomitant significant alteration of activity.[133] Porous polymeric CN nanosheets have been recently developed through the in situ lithium chloride ions intercalation in dicyandiamide polycondensation process using a stepwise thermal treatment (Figure 15).[131] Compared with the bulk-CN, the CN-nanosheets presented higher surface

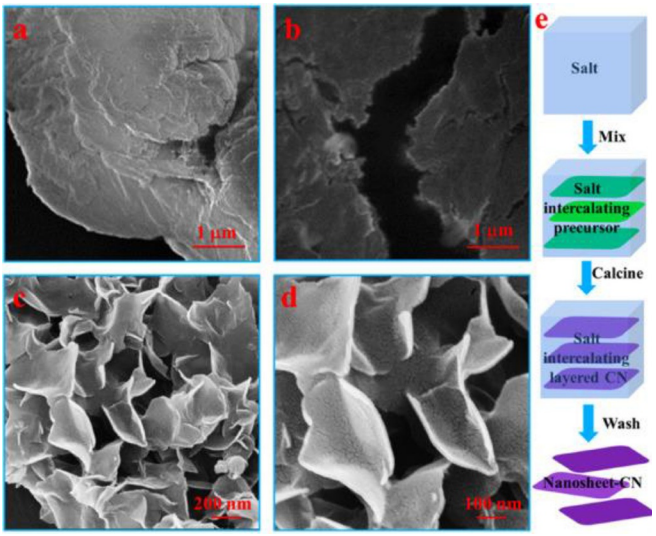

Figure 15. SEM image of a) bulk-CN, b) bulk-CN/Li^+ Cl^-, c) nanosheet-CN and d) the nanosheets corresponding height image, e) schematic of uniform CN nanosheets synthesis through water assisted exfoliation complex of 2D CNs and metal salt. Reprinted from Ref. [131] with permission from Elsevier.

area, superior e^- mobility increasing their lifetime, higher E_g enhancing redox ability and reduced charge carriers recombination rates. The synergy of these properties resulted in a six-fold increase of H_2 production under visible light irradiation.

Using a top-down synthesis approach, CN nanosheets have been developed from the thermal oxidation etching of bulk CN under air.[134] The thickness of CN nanosheets can be fine-tuned through the controlled thermal treatment (Figure 16). Compared with the bulk CN, CN nanosheets showed larger surface area, increased E_g, improved electron transport ability along the in-plane direction and prolonged lifetime of charge carriers, presenting increased hydrogen production. The actual temperature of the thermal treatment may have critical effect on both the optical properties and the morphology. Chen et al.

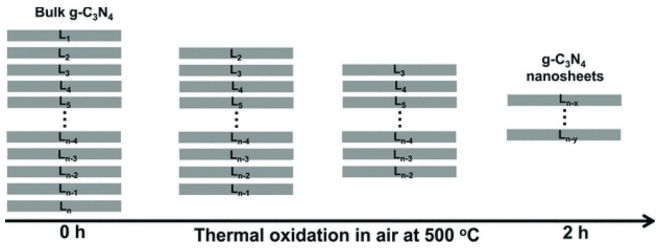

Figure 16. Schematic of the formation process of the g-C_3N_4 nanosheets by thermal oxidation etching of bulk g-C_3N_4 at 500 °C in air. Reproduced with permission from Ref. [134] Copyright 2012, Wiley-VCH.

using a two-step thermal condensation of melamine reported that processing temperatures higher than 650 °C induce a blue shift of the absorption edge, owing to the quantum size confinement effect and an absorption peak near 500 nm associated with n–π* transitions.[135] At the same time, thermal treatment at high temperatures also allowed the fabrication of atomically thin structure-distorted CN nanosheets. Structural distortion has been also achieved through the control of the atmosphere during the thermal process. Ho et al. reported that under H_2 atmosphere structural distortion can be achieved through the formation of amino groups within the g-C_3N_4 structure and the subsequent generation of strong hydrogen bonding interaction between layers.[136] The distorted structure resulted in n–π* transitions allowing increased visible-light absorption. In a recent study, Kang et al. presented the significance of amorphous phase CN (ACN) in photoactivity.[137] In general, amorphous phase materials are not preferred in photocatalysis due to the lack of long-range atomic ordering and the presence of many defects, properties that affect the diffusion of charge carriers. However, the development of ACN through a post-heating treatment of partially crystalline CN at 620 °C under Ar atmosphere, resulted in a significant narrowing of the band gap (1.9 eV), shifting the absorption edges from 460 to 682 nm. Under these conditions, the unaltered strong C–N bonds in the tri-*s*-triazine units retained the short-range atomic order, whereas the rupture of the relatively weak intra-layer and in-plane H-bonding and van der Waals forces disturbed the planar cohesion and weaken the inter-planar interaction, affecting the long-range atomic order. The ACN presented superior photocatalytic H_2 production compared with the CN under pure visible light irradiation, ≈12.5 times. It should be noted that usually thermal treatments at high temperatures result in improved crystallinity as demonstrated for solid materials with strong bonds, for example, metal oxides.[138] However, electrostatic interactions such as hydrogen bonding and van der Waals forces play a key role for maintaining the long-range atomic order and therefore the 2D or 3D structure of CN. Disrupting these weak interactions can alter in a reverse way the crystallinity of CN materials. This study is in agreement with recent evidence of the enhanced photoactivity of low molecular weight CN comprised of isolated oligomers of melem.[139]

On the other hand, low-defected and highly condensed CN photocatalysts, prepared through controlled thermal treatment in the presence of NH_3, increased photocatalytic H_2 production.[140] Using a simple thermal treatment under controlled atmosphere, Liang et al. modified the morphology and the chemical structure of bulk CN, resulting in the formation of CN nanosheets with abundant in-plane holes and carbon vacancies.[141] The authors observed an increase of the E_g energy, broader light absorption in the visible and near-infrared region, modification of the band edge potentials and improved charge separation efficiency. The resulted self-modified with carbon vacancies CN nanosheets presented more exposed active edges and a nearly 20 times higher H_2 production rates compared with the corresponding bulk CN.

Isotype CN heterojunctions have been developed through the coupling of CN nanostructures in a two-step synthesis process.[142] The energy difference of the band edges levels resulted in the formation of a Type II heterojunction, favoring the migration and separation of the photogenerated charges and therefore improving photoactivity. Openly-structured CN microspheres were developed by a simple controlled crystallization strategy using CN nanosheets as precursor, presenting superior photoactivity compared with bulk and CN nanosheets.[143] CN nanorods although presenting small specific surface have been proven more active than bulk and mesoporous CN presumably due to the higher charge separation efficiency in the two-dimensional layered structure.[144] Strategies targeting on controlling the morphology, increasing the surface area and tuning the band structure by controlling the nanostructure or using templating techniques have been also shown beneficial for photocatalytic H_2 generation.[144,145] Properties such as, structure, morphology, porosity, surface area, and light harvesting can be easily tuned by hard- and soft-templating methods, using for example silica nanoparticles or ionic liquids and surfactants. In addition, supramolecular preassembled structures using a variety of molecular structures as the starting monomers has been also shown an effective strategy to control key parameters of the photocatalyst.[146] All these examples demonstrate the unconstrained with respect to inorganic SCs modification of CN, a factor that originates from the polymeric nature of CN.

CN has been also effectively coupled with a variety of inorganic nanomaterials including metal nanoparticles, oxides, hydroxides, and sulfides.[147] Studies focused mostly on improving light absorption properties and charge carriers separation. Photocatalytic H_2 production was drastically increased by the coupling of CN with traditional inorganic SCs such as CdS[147a] and TiO_2.[149] The enhanced activity was attributed primarily to efficient separation of photogenerated e^-/h^+ pairs, owing to the difference in the CB and VB edge potential of the two parts, as well as to morphological properties. The improved H_2 production rates from ternary composites made of g-C_3N_4, TiO_2, and MnO_x, using Pt as cocatalyst and isopropanol as sacrificial agent has been attributed to a synergistic effect linked with charge separation.[150] The differences of the actual band structure in TiO_2 and g-C_3N_4 drove e^- and h^+ into opposite directions while the presence of MnO_x further increased h^+ migration and transfer. Noble-metal free CN-based nanomaterials have been also proven active. In this regard, hybrid CN/$Co(OH)_2$ nanocomposites co-sensitized with dyes have been

developed,[147d] whereas Li et al. deposited nanoflower-structured MoS_2 on pyridine-modified CN.[151] Impressive apparent quantum efficiencies were reported at 520 and 550 nm, 29.6 and 27.3 % respectively.[147d]

The junction of CN with carbon nanostructures has been also investigated.[148,152] Chen et al. coupled CN with multi-walled carbon nanotubes (CNT).[152b] The superior photocatalytic activity of the prepared g-C_3N_4/CNT materials under visible light was ascribed to the reduction of the population distribution of short-lived and increasing the percentage of long-lived charges. Nanocomposites of mesoporous CN coupled with carbon nanotubes (CNT) were also hybridized with NiS.[152d] The enhanced H_2 production under visible light was ascribed to the formation of a Schottky-type junction between CN and CNT, promoting the migration of photoinduced e^- to the conductive CNT and finally on the NiS cocatalyst. Similarly, a 3.7-fold increase in H_2 photoproduction from aqueous methanol solution was observed using CNT(2 wt %)/CN composites compared with the pure CN ascribed to the efficient transfer of e^- to CNT (Figure 17).[148] Besides the efficient charge separation, Suryawanshi et al. suggested also that morphological changes in CN induced by the presence of CNT may also affect the photocatalytic activity. In their composites, the optimum CNT content was 0.5 wt % for H_2 production using methanol as sacrificial agent.[152c] The formation of a stable CN colloidal suspension through protonation and depolymerization reactions of bulk CN under strong oxidizing conditions was used as the CN precursor for the development of CN@CNT composites and the subsequent fabrication of thin-film electrodes.[152e] A polymer-based heterostructure was observed through the wrapping of the CNT with CN in which CNT functioned as an efficient pathway for e^- transport allowing fast charge separation. The coupling CN with carbon nanodots (CDs) resulted in an efficient photocatalysts able to catalyze the overall WS reaction presenting a remarkable stability for more than 200 cycles.[153] Without using any sacrificial agent, a H_2/O_2 molar ratio identical to the theoretical value of 2 for pure WS was observed under pure visible light irradiation. In these materials, CDs were proven to have an active participation in catalysis. The reaction proceeded via H_2O oxidation to H_2O_2 followed H_2O_2 disproportionation to O_2, the second step being catalyzed by CDs.

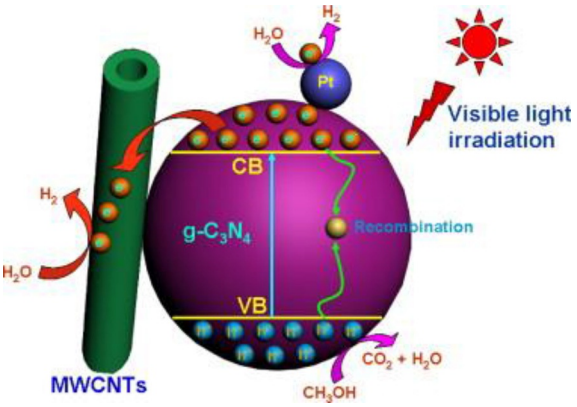

Figure 17. Schematic of photogenerated charge carrier's separation and transfer in the MWNTs/g-C_3N_4 system under visible light irradiation. Reprinted from Ref. [148] with permission from Elsevier.

5.2. Other CNSs containing materials

In addition to carbon nitride, nanomaterials containing other CNSs have been also used in H_2 photoproduction. Here, CNSs have been used as support of photoactive materials for the development of nanocomposites applied in photocatalytic reactions. CNSs have been reported to exhibit cooperative or synergetic effects. Many studies made use of the unique properties of CNSs such as the high electron conductivity, large electron storage capacity, large surface area, light absorption ability and morphology in order to improve key parameters that control activity. CNTs and graphene (Gr) are the most commonly used carbon nanostructures.[154] In this type of materials the most important issues that must be solved are related with the homogeneous coverage of the support and the formation of tight interface between the two parts. Different strategies have been adopted for the development of hybrid nanocomposites including in situ strategies, solution and solid-state approaches, using either bare or even functionalized CNTs.[154a,155] Regarding the effect of CNSs in the photocatalytic mechanism, a similar analogy to the CN-based composites is obtained. Photoexcited e^- flow from the SC into the CNTs in order to align the different Fermi levels. Efficient charge separation is ensured due to the high conductivity and large electron storage capacity. Again, intimate coupling of the difference phases must be obtained to allow charge migration and transportation. CNSs may also act as photosensitizers extending the absorption region of light to higher wavelengths. In some cases this was explained through the introduction of intermediate states.[156] In addition, the high surface area of most CNSs facilitates the dispersion of nanoparticles (crucial in suspension systems) and may control particle size offering high nucleation sites.[157]

Graphene nanosheets were decorated with CdS clusters and applied for H_2 production using Pt as cocatalyst and lactic acid as sacrificial agent.[158] A 5 times increase in activity was observed with an apparent quantum efficiency of 22.5 % at wavelength of 420 nm. The enhanced catalytic activity was attributed primarily to the presence of Gr. Under light irradiation, the excited e^- on the CdS CB are transferred to 1) Pt deposited on the surface of CdS clusters, 2) carbon atoms on the Gr sheets or 3) Pt located on the Gr nanosheets (Figure 18). The authors suggested that Gr served as an electron collector and transporter, separating efficiently the photogenerated charges. Noble-metal free nanocatalysts prepared through the coupling of CdS with Gr have been shown to present comparable H_2 generation efficiency with systems containing Pt as cocatalyst.[160] Gr was suggested having a similar role as Pt nanoparticles, accepting and transferring electrons, functioning as an effective H_2 evolution promoter for CdS.

An interesting study by Li et al. presented the development of ternary systems, through the controlled photodeposition of MoS_2 nanosheets on composites made of reduced graphene

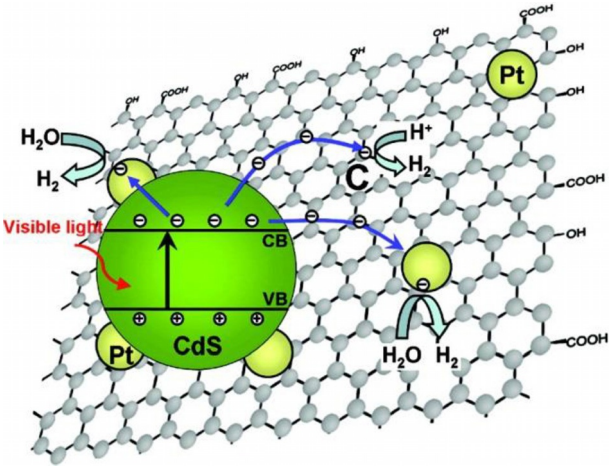

Figure 18. Schematic illustration of the charge separation and transfer in the graphene/CdS system under visible light. Reprinted with permission from Ref. [158]. Copyright (2011) American Chemical Society.

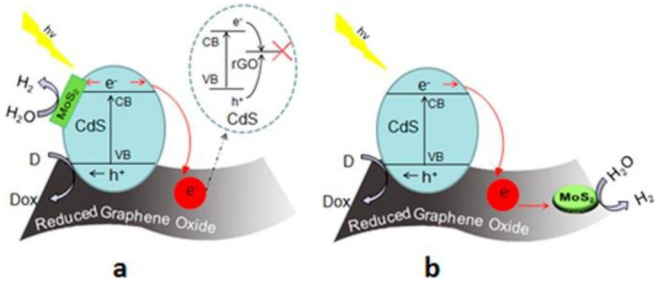

Figure 19. Schematic illustration of incompatibility between the photoexcited e^- transfer from CdS to rGO and the hydrogen evolution reaction at MoS_2 for MoS_2 sheets developed on a) CdS, b) rGO. Reprinted with permission from Ref. [159]. Copyright (2014) American Chemical Society.

oxide and CdS (rGO/CdS).[159] The authors, simply by changing the pH of the synthesis solution were able to tune the deposition of MoS_2 on either the surface of the CdS particles or the exposed rGO (Figure 19). Materials where MoS_2 were developed on rGO presented superior H_2 production under visible light irradiation. rGO acted as acceptor of the photoexcited e^- formed in CdS and effectively transferred them on MoS_2. On the contrary, when MoS_2 were loaded on CdS, photoexcited e^- injected into rGO could not be transferred on the MoS_2 active site, resulting in lower activity (Figure 19a). Yang et al. demonstrated the effect of preparation method on the morphology and activity of similar ternary systems (Gr/CdS/MoS_2).[61c] Materials prepared through the photodeposition of MoS_2 on Gr/CdS were proven significantly more active than the materials prepared through hydrothermal treatment. An important improvement on the photostability was also observed. Compared with the typical layered layer MoS_2 structure, the photodeposition method induced morphological and structural transformation resulting in small MoS_2 particles homogeneously dispersed on Gr/CdS. The small MoS_2 particles provided more catalytic active sites and shorter charge-transfer distance than the layered structure, improving H_2 production and h^+ consumption by the sacrificial agent used.

Nanocomposites of TiO_2 and rGO have been developed and applied in H_2 production from aqueous solution of different alcohols.[162] The ratio and the contact of the two parts were optimized using several synthesis techniques. Materials prepared by the hydrothermal method exhibited the best performance. Strong interaction between TiO_2 nanoparticles and rGO is mandatory for enhanced photocatalytic activity, suppressing recombination rates and providing charge separation. This was the main factor for the increased H_2 production from $ZnIn_2S_4$/rGO nanocomposites.[163] In addition, the introduction of surface plasmon resonance (SPR) phenomena in metal oxide/ graphene nanocomposites has been investigated. Ag-TiO_2-graphene ternary nanocomposites presented increased H_2 photoproduction from a water/ethanol (10 vol.%) solution.[164] rGO induced improvements in light absorption intensity, extending light absorption range and enhancing charge carriers transportation while the presence of Ag nanoparticles added SPR effects. In addition to the traditional particles-on-sheet geometry where metal oxide nanoparticles are deposited on graphene sheets, core/shell rGO/TiO_2 composite were also prepared.[165] Under UV light irradiation, and using methanol as sacrificial agent, the core/shell structures presented higher photoactivity due to the increased contact between the two parts. Besides acting simply as charge separator, graphene has been also shown to modify the electronic band structure of metal oxides.

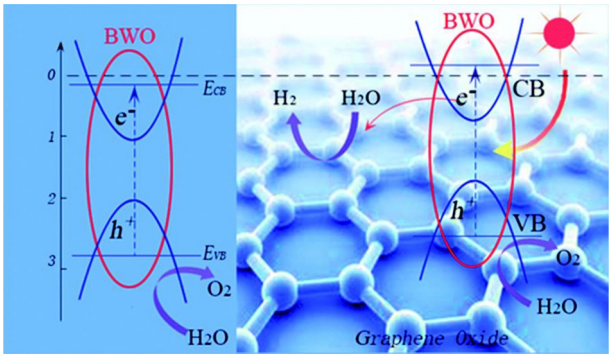

Figure 20. Schematic representation of the Bi_2WO_6 (left side) and the Gr-Bi_2WO_6 band edges energy level and the mechanism of the photocatalytic WS process. Reproduced from Ref. [161] with permission from The Royal Society of Chemistry.

Sun et al. demonstrated using Mott-Schottky plots that the coupling of Bi_2WO_6 with rGO can significant up-shift the CB of the metal oxide at more negative values (Figure 20). This allowed H_2 production from aqueous methanol solution under visible light irradiation.[161]

Less explored metal oxides have been also coupled with CNSs. ZnO nanorods have been effectively developed on rGO.[46c] Factors related with charge separation, the actual 1D morphology that favored the directional transfer of e^- and the strong ZnO-rGO interaction expressed as C-*O*-Zn linkage, affected significantly the photocatalytic H_2 production from aqueous glycerol solution. Through the development of different ZnO nanoparticles Kang et al. reported the crucial effect of

morphology on the photoactivity of ZnO/rGO nanocomposites.[169] 1D nanoparticles presented higher transfer rates of photoexcited e^- from ZnO to rGO resulting in enhanced activity. More sophisticated ZnO@ZnS-Bi_2S_3 core–shell nanorods anchored on rGO further enhanced H_2 photoproduction from aqueous glycerol solution, owing to improvements in light absorption and charge handling properties.[171]

Dye-sensitized CNT[170,172] and rGO[173] have been also reported as efficient catalysts for H_2 production under visible light irradiation. Simply by mixing bare or oxidized CNT with Eosin Y dye and using Pt as cocatalyst the enhanced catalytic activity with an apparent quantum yield of 12.14% was attributed to the trapping of photogenerated electrons by CNT.[172] CNT increased significantly the fraction of photogenerated e^- converted into H_2 suggesting a CNT-catalytic H_2 production while the presence of Pt enhanced the dye stability under working conditions (Figure 21).[170]

Table 1 summarizes the photocatalytic H_2 production over different CN-based and CNSs containing catalysts (hybrids, heterojunctions) under various catalytic conditions including the cocatalyst, sacrificial agent, light source, amount of the catalyst used and H_2 generation rate. Although these H_2 evolution rates cannot be compared,[58] from the data in Table 1 can be concluded that activity is greatly affected by many factors. Properties such as the light source, cocatalyst, sacrificial agent can be easily controlled. However, the synthesis process that eventually controls the properties of the material seems to be the key parameter controlling activity.

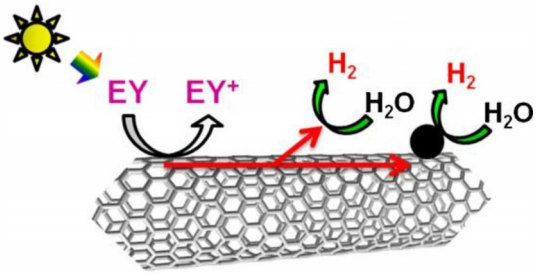

Figure 21. Schematic illustration of CNT sensitized with Eosin Y. Reprinted from Ref. [170] with permission from Elsevier.

Table 1. Photocatalytic H_2 production rate over different CN, CN hybrid, and CNSs hybrid photocatalysts.

Photocatalyst	Cocatalyst [wt%]	Sacrificial reagents	Catalyst amount [mg]	Light	H_2 rate [$\mu mol\,h^{-1}$]	Ref.
Pure CN						
CN NS	Pt (6)	TEOA	50	UV/vis	170.5	[134]
CN NS	Pt (6)	TEOA	50	visible	≈30	[134]
CN NS	Pt (3)	TEOA	50	visible	177	[135]
ACN	Pt (6)	TEOA	50	visible	≈7.9	[137]
LMW CN	Pt (8)	methanol	20	visible	≈5.4	[139]
CN	Pt (3)	TEOA	50	visible	303	[140]
CN NS	Pt (3)	TEOA	10	visible	82.9	[141]
CN microspheres	Pt (3)	TEOA		visible	392	[143]
CN NS	Pt (3)	TEOA	20	visible	230	[166]
CN Hybrids						
CdS	Pt (1)	ethanol	100	visible	17.27	[147a]
TiO_2	–	methanol	100	UV/vis	52.71	[149]
TiO2	Pt (1)	TEOA	100	visible	178	[167]
TiO_2-MnO_x	Pt (1)	isopropanol		UV/Vis	7.5	[150]
MoS_2	–	TEOA	50	visible	25	[151]
CN/CNSs						
CNTs	Pt (1)	methanol	100	visible	7.58	[148]
CNTs	Pt (1.2)	TEOA	100	visible	≈39.4	[152b]
CNTs	NiS (1)	TEOA	50	visible	≈26.5	[152d]
Gr QD	Pt (3)	TEOA	20	visible	≈43.6	[152a]
CDs	–	–	80	visible	8.4	[153]
CNSs Hybrids						
Gr/CdS	Pt (0.5)	lactic acid	20	visible	1120	[158]
Gr/CdS	–	Na_2S/Na_2SO_3	30	>380 nm	≈5	[160]
GO/CdS	Pt	methanol	50	UV/vis	≈110	[168]
rGO/CdS/MoS_2	–	lactic acid	50	visible	99	[159]
Gr/CdS/MoS_2	–	lactic acid	40	visible	513	[61c]
rGO/TiO_2 (P25)	–	methanol	100	UV/Vis	≈110	[162]
rGO/ZnIn2S4	–	lactic acid	50	Visible	≈41	[163]
rGO/TiO_2	Pt (0.05)	methanol		UV	50	[165]
rGO/Bi_2WO_6	–	lactic acid	30	visible	159.20	[161]
rGO/ZnO	–	ethanol/TEOA	25	UV/Vis	≈14.5	[169]

6. Conclusions

In the last few decades the photocatalytic approach has turned out to be one of the most challenging candidates for sustainable future energy production. The great interest shown by the scientific community has been expressed in the application of numerous photoactive materials and various catalytic conditions. These two parameters hold the key for efficient H_2 production. The use of renewable organic sacrificial agents has been proven to have more practical industrial application compared to the pure water spitting process, at least at medium term.

The challenge is to develop stable and efficient catalysts that can harvest solar light. An important issue that must be addressed is the development of cocatalysts, preferentially without using precious materials for smooth scale-up synthesis and practical applications. Recent advantages in materials synthesis allowed the development of novel nanostructures with exotic structures, multi-phase composition and precise control of morphology at the nanoscale. In addition to visible-light absorption, materials should be able to address several other issues, the most important of which seems the charge recombination process. Among the different strategies applied, the coupling of novel or even known materials for the development of multi-phase nanostructures through the synthesis of heterostructures, heterojunctions/ homojunctions, has been proven in many cases beneficial for H_2 photoproduction and it appears that has great promise in this field. In this aspect, instead of optimizing the properties of a single component, the properties of different materials (or even different phases) can be coupled towards optimizing photoactivity. Care must be given in the choice of the proper materials. Deep understanding of the individual components is required but in some cases it is still challenging. Rational design of integrated engineering processes that include interface engineering, control of the composition, structure and morphology at the nanoscale must be developed. In the case of junctions, the individual materials must possess correctly positioned and alighted band edges for a feasible and spontaneous intra- and intercharge transfer. In the case of heterostructures, semiconductors can be coupled with highly conductive materials such as carbon nanostructures. Both cases will provide the requested driving force for charge separation, probably the parameter of the greatest importance in photocatalysis. In addition, plasmonic nanoparticles, such as Ag and Au nanoparticles, hold also great potential. LSPR provides improved absorption of visible light but also enhancing in parallel charge separation. These characteristics improve the inherent limitations of traditional SC photocatalysts.

The limitations of SCs and the latest results presented in this Review dictate the direction of future efforts. Future research should be primarily directed on the development of effective paths for e^- transportation to H_2 evolution sites, separated from h^+ collection regions, without compromising other properties. It is clear, therefore, that novel synthetic strategies are required to fine-tune all critical properties for enhanced H_2 evolution. In this Review we went through the most used photocatalysts and we focused on the latest advances on CN- and CNSs-based materials for the development of hybrid and full-organic nanostructures applied in H_2 photoproduction. It appears that not only the nature but also the synthesis approach affects greatly the morphology and phase composition at the nanoscale, allowing control of specific key properties. Based on the increasing number of contributions in the literature and the impressive improvement in H_2 production achieved within few years especially under visible light irradiation, it seems there is a lot of room for improvement in this specific category of nanomaterials towards enhanced activity.

Acknowledgements

K.C.C. acknowledges the TALENTS FVG Programme for a Postdoctoral fellowship funded from the European Social Fund (Operational Programme 2007–2013, Objective 2 Regional Competitiveness and Employment, Axis 5 Transnational cooperation, TALENTS FVG Programme).

Keywords: hydrogen · photocatalysis · photoreforming · renewable energy · water splitting

[1] N. S. Lewis, D. G. Nocera, *Proc. Natl. Acad. Sci. USA* **2006**, *103*, 15729–15735.
[2] M. Ni, D. Y. C. Leung, M. K. H. Leung, K. Sumathy, *Fuel Process. Technol.* **2006**, *87*, 461–472.
[3] M. H. Halabi, M. H. J. M. de Croon, J. van der Schaaf, P. D. Cobden, J. C. Schouten, *Appl. Catal. A* **2010**, *389*, 68–79.
[4] C. A. Rodriguez, M. A. Modestino, D. Psaltis, C. Moser, *Energy Environ. Sci.* **2014**, *7*, 3828–3835.
[5] K. H. A. Fujishima, *Nature* **1972**, *238*, 37–38.
[6] S. Zinoviev, F. Muller-Langer, P. Das, N. Bertero, P. Fornasiero, M. Kaltschmitt, G. Centi, S. Miertus, *ChemSusChem* **2010**, *3*, 1106–1133.
[7] I. Rossetti, *ISRN Chem. Eng.* **2012**, *2012*, 1–21.
[8] a) L. Yuan, C. Han, M.-Q. Yang, Y.-J. Xu, *Int. Rev. Phys. Chem.* **2016**, *35*, 1–36; b) M. G. Walter, E. L. Warren, J. R. McKone, S. W. Boettcher, Q. Mi, E. A. Santori, N. S. Lewis, *Chem. Rev.* **2010**, *110*, 6446–6473; c) X. Chen, S. Shen, L. Guo, S. S. Mao, *Chem. Rev.* **2010**, *110*, 6503–6570; d) S. J. A. Moniz, S. A. Shevlin, D. J. Martin, Z.-X. Guo, J. Tang, *Energy Environ. Sci.* **2015**, *8*, 731–759.
[9] A. V. Puga, *Coord. Chem. Rev.* **2016**, *315*, 1–66.
[10] H. Y. Y. Taniguchi, H. Tamura, *Chem. Lett.* **1983**, *10*, 269–272.
[11] N. Luo, Z. Jiang, H. Shi, F. Cao, T. Xiao, P. Edwards, *Int. J. Hydrogen Energy* **2009**, *34*, 125–129.
[12] J. C. Colmenares, A. Magdziarz, M. A. Aramendia, A. Marinas, J. M. Marinas, F. J. Urbano, J. A. Navio, *Catal. Commun.* **2011**, *16*, 1–6.
[13] A. Patsoura, D. I. Kondarides, X. E. Verykios, *Catal. Today* **2007**, *124*, 94–102.
[14] A. Fujishima, X. Zhang, D. Tryk, *Surf. Sci. Rep.* **2008**, *63*, 515–582.
[15] T. Kawai, T. Sakata, *J. Chem. Soc. Chem. Commun.* **1980**, 694–695.
[16] T. Sakata, T. Kawai, *Chem. Phys. Lett.* **1981**, *80*, 341–344.
[17] T. Kawai, T. Sakata, *Nature* **1980**, *286*, 474–476.
[18] T. Kawai, T. Sakata, *Chem. Lett.* **1981**, *81*, 81–84.
[19] K. Hashimoto, T. Kawai, T. Sakata, *J. Phys. Chem.* **1984**, *88*, 4083–4088.
[20] S. Sato, J. M. White, *J. Am. Chem. Soc.* **1980**, *102*, 7206–7210.
[21] S. Sato, J. M. White, *Chem. Phys. Lett.* **1980**, *70*, 131–134.
[22] H. Harada, T. Sakata, T. Ueda, *J. Am. Chem. Soc.* **1985**, *107*, 1773–1774.
[23] G. L. Chiarello, M. H. Aguirre, E. Selli, *J. Catal.* **2010**, *273*, 182–190.
[24] A. Naldoni, M. D'Arienzo, M. Altomare, M. Marelli, R. Scotti, F. Morazzoni, E. Selli, V. Dal Santo, *Appl. Catal. B* **2013**, *130–131*, 239–248.
[25] a) T. Chen, Z. Feng, G. Wu, J. Shi, G. Ma, P. Ying, C. Li, *J. Phys. Chem. C* **2007**, *111*, 8005–8014; b) J. G. Highfield, M. H. Chen, P. T. Nguyen, Z. Chen, *Energy Environ. Sci.* **2009**, *2*, 991; c) O. I. Micic, Y. Zhang, K. R. Cro-

mack, A. D. Trifunac, M. C. Thurnauer, *J. Phys. Chem.* **1993**, *97*, 13284 – 13288.
[26] G. L. Chiarello, D. Ferri, E. Selli, *J. Catal.* **2011**, *280*, 168 – 177.
[27] H. J. Choi, M. Kang, *Int. J. Hydrogen Energy* **2007**, *32*, 3841 – 3848.
[28] N. Strataki, V. Bekiari, D. I. Kondarides, P. Lianos, *Appl. Catal. B* **2007**, *77*, 184 – 189.
[29] C.-Y. Wang, H. Groenzin, M. J. Shultz, *J. Am. Chem. Soc.* **2004**, *126*, 8094 – 8095.
[30] a) J. Chen, D. F. Ollis, W. H. Rulkens, H. Bruning, *Water Res.* **1999**, *33*, 669 – 676; b) M. T. Uddin, O. Babot, L. Thomas, C. Olivier, M. Redaelli, M. D'Arienzo, F. Morazzoni, W. Jaegermann, N. Rockstroh, H. Junge, T. Toupance, *J. Phys. Chem. C* **2015**, *119*, 7006 – 7015; c) C. Gomes Silva, R. Juárez, T. Marino, R. Molinari, H. García, *J. Am. Chem. Soc.* **2011**, *133*, 595 – 602.
[31] J. Schneider, D. W. Bahnemann, *J. Phys. Chem. Lett.* **2013**, *4*, 3479 – 3483.
[32] H. Bahruji, M. Bowker, P. R. Davies, D. J. Morgan, C. A. Morton, T. A. Egerton, J. Kennedy, W. Jones, *Top. Catal.* **2015**, *58*, 70 – 76.
[33] a) A. V. Puga, A. Forneli, H. García, A. Corma, *Adv. Funct. Mater.* **2014**, *24*, 241 – 248; b) S. Yang, H. Wang, H. Yu, S. Zhang, Y. Fang, S. Zhang, F. Peng, *Int. J. Hydrogen Energy* **2016**, *41*, 3446 – 3455; c) S. Y. Ryu, W. Balcerski, T. K. Lee, M. R. Hoffmann, *J. Phys. Chem. C* **2007**, *111*, 18195 – 18203.
[34] a) Y. Yang, C. Chang, H. Idriss, *Appl. Catal. B* **2006**, *67*, 217 – 222; b) S. Kundu, A. B. Vidal, M. A. Nadeem, S. D. Senanayake, H. Idriss, P. Liu, J. A. Rodriguez, D. Stacchiola, *J. Phys. Chem. C* **2013**, *117*, 11149 – 11158.
[35] Z. Jin, Q. Lin, X. Zheng, C. Xi, C. Wang, H. Zhang, L. Feng, H. Wang, Z. Chen, Z. Jiang, *J. Photochem. Photobiol. A* **1993**, *71*, 85 – 96.
[36] a) T. Montini, V. Gombac, L. Sordelli, J. J. Delgado, X. Chen, G. Adami, P. Fornasiero, *ChemCatChem* **2011**, *3*, 574 – 577; b) M. J. Sampaio, J. W. L. Oliveira, C. I. L. Sombrio, D. L. Baptista, S. R. Teixeira, S. A. C. Carabineiro, C. G. Silva, J. L. Faria, *Appl. Catal. A* **2016**, *518*, 198 – 205; c) A. Gallo, T. Montini, M. Marelli, A. Minguzzi, V. Gombac, R. Psaro, P. Fornasiero, V. Dal Santo, *ChemSusChem* **2012**, *5*, 1800 – 1811; d) I. Romero Ocaña, A. Beltram, J. J. Delgado Jaén, G. Adami, T. Montini, P. Fornasiero, *Inorg. Chim. Acta* **2015**, *431*, 197 – 205.
[37] D. I. Kondarides, V. M. Daskalaki, A. Patsoura, X. E. Verykios, *Catal. Lett.* **2008**, *122*, 26 – 32.
[38] M. Cargnello, T. Montini, S. Y. Smolin, J. B. Priebe, J. J. Delgado Jaen, V. V. Doan-Nguyen, I. S. McKay, J. A. Schwalbe, M. M. Pohl, T. R. Gordon, Y. Lu, J. B. Baxter, A. Bruckner, P. Fornasiero, C. B. Murray, *Proc. Natl. Acad. Sci. USA* **2016**, *113*, 3966 – 3971.
[39] K. Shimura, H. Yoshida, *Energy Environ. Sci.* **2011**, *4*, 2467.
[40] a) G. Carraro, C. Maccato, A. Gasparotto, T. Montini, S. Turner, O. I. Lebedev, V. Gombac, G. Adami, G. Van Tendeloo, D. Barreca, P. Fornasiero, *Adv. Funct. Mater.* **2014**, *24*, 372 – 378; b) Y. Li, J. Wang, S. Peng, G. Lu, S. Li, *Int. J. Hydrogen Energy* **2010**, *35*, 7116 – 7126; c) R. M. Mohamed, E. S. Aazam, *Chin. J. Catal.* **2012**, *33*, 247 – 253; d) G. Iervolino, V. Vaiano, D. Sannino, L. Rizzo, P. Ciambelli, *Int. J. Hydrogen Energy* **2016**, *41*, 959 – 966; e) D. V. Esposito, R. V. Forest, Y. Chang, N. Gaillard, B. E. McCandless, S. Hou, K. H. Lee, R. W. Birkmire, J. G. Chen, *Energy Environ. Sci.* **2012**, *5*, 9091 – 9099; f) D. Jing, M. Liu, J. Shi, W. Tang, L. Guo, *Catal. Commun.* **2010**, *12*, 264 – 267; g) X. Fu, X. Wang, D. Y. C. Leung, W. Xue, Z. Ding, H. Huang, X. Fu, *Catal. Commun.* **2010**, *12*, 184 – 187.
[41] M. R. St. John, A. J. Furgala, A. F. Sammells, *J. Phys. Chem.* **1983**, *87*, 801 – 805.
[42] M. Zhou, Y. Li, S. Peng, G. Lu, S. Li, *Catal. Commun.* **2012**, *18*, 21 – 25.
[43] X. Fu, J. Long, X. Wang, D. Leung, Z. Ding, L. Wu, Z. Zhang, Z. Li, X. Fu, *Int. J. Hydrogen Energy* **2008**, *33*, 6484 – 6491.
[44] A. Caravaca, W. Jones, C. Hardacre, M. Bowker, *Proc. R. Soc. London Ser. A* **2016**, *472*, 20160054.
[45] a) F. Ma, M. A. Hanna, *Bioresour. Technol.* **1999**, *70*, 1 – 15; b) V. M. Daskalaki, D. I. Kondarides, *Catal. Today* **2009**, *144*, 75 – 80.
[46] a) X. Fu, X. Wang, D. Y. C. Leung, Q. Gu, S. Chen, H. Huang, *Appl. Catal. B* **2011**, *106*, 681 – 688; b) M. P. Languer, F. R. Scheffer, A. F. Feil, D. L. Baptista, P. Migowski, G. J. Machado, D. P. de Moraes, J. Dupont, S. R. Teixeira, D. E. Weibel, *Int. J. Hydrogen Energy* **2013**, *38*, 14440 – 14450; c) R. Lv, X. Wang, W. Lv, Y. Xu, Y. Ge, H. He, G. Li, X. Wu, X. Li, Q. Li, *J. Chem. Technol. Biotechnol.* **2015**, *90*, 550 – 558.
[47] a) V. M. Daskalaki, P. Panagiotopoulou, D. I. Kondarides, *Chem. Eng. J.* **2011**, *170*, 433 – 439; b) A. Petala, E. Ioannidou, A. Georgaka, K. Bourikas, D. I. Kondarides, *Appl. Catal. B* **2015**, *178*, 201 – 209.
[48] a) P. Panagiotopoulou, E. E. Karamerou, D. I. Kondarides, *Catal. Today* **2013**, *209*, 91 – 98; b) F. Pompeo, G. F. Santori, N. N. Nichio, *Catal. Today* **2011**, *172*, 183 – 188; c) V. Augugliaro, H. A. H. El Nazer, V. Loddo, A. Mele, G. Palmisano, L. Palmisano, S. Yurdakal, *Catal. Today* **2010**, *151*, 21 – 28.
[49] J. Kim, D. Monllor-Satoca, W. Choi, *Energy Environ. Sci.* **2012**, *5*, 7647.
[50] M. Bowker, P. R. Davies, L. S. Al-Mazroai, *Catal. Lett.* **2009**, *128*, 253 – 255.
[51] a) J. Kim, W. Choi, *Energy Environ. Sci.* **2010**, *3*, 1042; b) J. Kim, J. Lee, W. Choi, *Chem. Commun.* **2008**, 756 – 758.
[52] a) Y. Li, G. Lu, S. Li, *Chemosphere* **2003**, *52*, 843 – 850; b) Y. Li, G. Lu, S. Li, *Appl. Catal. A* **2001**, *214*, 179 – 185; c) Y. Li, Y. Xie, S. Peng, G. Lu, S. Li, *Chemosphere* **2006**, *63*, 1312 – 1318.
[53] a) A. Patsoura, D. I. Kondarides, X. E. Verykios, *Appl. Catal. B* **2006**, *64*, 171 – 179; b) J. Kim, Y. Park, H. Park, *Int. J. Photoenergy* **2014**, *2014*, 1 – 9.
[54] C. Liu, Z. Lei, Y. Yang, Z. Zhang, *Water Res.* **2013**, *47*, 4986 – 4992.
[55] a) A. Speltini, M. Sturini, F. Maraschi, D. Dondi, G. Fisogni, E. Annovazzi, A. Profumo, A. Buttafava, *Int. J. Hydrogen Energy* **2015**, *40*, 4303 – 4310; b) M. I. Badawy, M. Y. Ghaly, M. E. M. Ali, *Desalination* **2011**, *267*, 250 – 255.
[56] A. T. Garcia-Esparza, K. Takanabe, *J. Mater. Chem. A* **2016**, *4*, 2894 – 2908.
[57] T. A. Kandiel, K. Takanabe, *Appl. Catal. B* **2016**, *184*, 264 – 269.
[58] M. Qureshi, K. Takanabe, *Chem. Mater.* **2016**, DOI: 10.1021/acs.chemmater.6b02907.
[59] R. Abe, K. Hara, K. Sayama, K. Domen, H. Arakawa, *J. Photochem. Photobiol. A* **2000**, *137*, 63 – 69.
[60] a) T. Peng, X. Zhang, P. Zeng, K. Li, X. Zhang, X. Li, *J. Catal.* **2013**, *303*, 156 – 163; b) X. Wang, W.-c. Peng, X.-y. Li, *Int. J. Hydrogen Energy* **2014**, *39*, 13454 – 13461; c) R. Peng, C. M. Wu, J. Baltrusaitis, N. M. Dimitrijevic, T. Rajh, R. T. Koodali, *Chem. Commun.* **2013**, *49*, 3221 – 3223.
[61] a) J. Hu, A. Liu, H. Jin, D. Ma, D. Yin, P. Ling, S. Wang, Z. Lin, J. Wang, *J. Am. Chem. Soc.* **2015**, *137*, 11004 – 11010; b) Y. P. Xie, Z. B. Yu, G. Liu, X. L. Ma, H.-M. Cheng, *Energy Environ. Sci.* **2014**, *7*, 1895; c) M.-Q. Yang, C. Han, Y.-J. Xu, *J. Phys. Chem. C* **2015**, *119*, 27234 – 27246.
[62] A. Kudo, Y. Miseki, *Chem. Soc. Rev.* **2009**, *38*, 253 – 278.
[63] H. Tran, K. Chiang, J. Scott, R. Amal, *Photochem. Photobiol. Sci.* **2005**, *4*, 565 – 567.
[64] a) J. Rodriguez, P. X. Thivel, E. Puzenat, *Int. J. Hydrogen Energy* **2013**, *38*, 6344 – 6348; b) J. Yu, L. Qi, M. Jaroniec, *J. Phys. Chem. C* **2010**, *114*, 13118 – 13125; c) W. Sun, S. Zhang, Z. Liu, C. Wang, Z. Mao, *Int. J. Hydrogen Energy* **2008**, *33*, 1112 – 1117.
[65] C. R. López, E. P. Melián, J. A. Ortega Méndez, D. E. Santiago, J. M. Doña Rodríguez, O. González Díaz, *J. Photochem. Photobiol. A* **2015**, *312*, 45 – 54.
[66] Y. Tamaki, A. Furube, M. Murai, K. Hara, R. Katoh, M. Tachiya, *J. Am. Chem. Soc.* **2006**, *128*, 416 – 417.
[67] M. Bowker, C. Morton, J. Kennedy, H. Bahruji, J. Greves, W. Jones, P. R. Davies, C. Brookes, P. P. Wells, N. Dimitratos, *J. Catal.* **2014**, *310*, 10 – 15.
[68] Z. H. N. Al-Azri, W.-T. Chen, A. Chan, V. Jovic, T. Ina, H. Idriss, G. I. N. Waterhouse, *J. Catal.* **2015**, *329*, 355 – 367.
[69] a) H. Bahruji, M. Bowker, P. R. Davies, L. S. Al-Mazroai, A. Dickinson, J. Greaves, D. James, L. Millard, F. Pedrono, *J. Photochem. Photobiol. A* **2010**, *216*, 115 – 118; b) H. Bahruji, M. Bowker, P. R. Davies, F. Pedrono, *Appl. Catal. B* **2011**, *107*, 205 – 209.
[70] J. B. Joo, R. Dillon, I. Lee, Y. Yin, C. J. Bardeen, F. Zaera, *Proc. Natl. Acad. Sci. USA* **2014**, *111*, 7942 – 7947.
[71] B. Zielinska, E. Borowiakpalen, R. Kalenczuk, *Int. J. Hydrogen Energy* **2008**, *33*, 1797 – 1802.
[72] A. L. Linsebigler, G. Lu, J. T. Yates, *Chem. Rev.* **1995**, *95*, 735 – 758.
[73] a) M. Bowker, L. Gilbert, J. Counsell, C. Morgan, *J. Phys. Chem. C* **2010**, *114*, 17142 – 17147; b) M. Bowker, L. Cookson, J. Bhantoo, A. Carley, E. Hayden, L. Gilbert, C. Morgan, J. Counsell, P. Yaseneva, *Appl. Catal. A* **2011**, *391*, 394 – 399; c) M. Bowker, H. Bahruji, J. Kennedy, W. Jones, G. Hartley, C. Morton, *Catal. Lett.* **2015**, *145*, 214 – 219.
[74] V. Subramanian, E. E. Wolf, P. V. Kamat, *J. Am. Chem. Soc.* **2004**, *126*, 4943 – 4950.

[75] H. B. Michaelson, *J. Appl. Phys.* **1977**, *48*, 4729.

[76] a) L. S. Al-Mazroai, M. Bowker, P. Davies, A. Dickinson, J. Greaves, D. James, L. Millard, *Catal. Today* **2007**, *122*, 46 – 50; b) H. Bahruji, M. Bowker, P. R. Davies, J. Kennedy, D. J. Morgan, *Int. J. Hydrogen Energy* **2015**, *40*, 1465 – 1471.

[77] X. Jiang, X. Fu, L. Zhang, S. Meng, S. Chen, *J. Mater. Chem. A* **2015**, *3*, 2271 – 2282.

[78] K. Wenderich, A. Klaassen, I. Siretanu, F. Mugele, G. Mul, *Angew. Chem. Int. Ed.* **2014**, *53*, 12476 – 12479; *Angew. Chem.* **2014**, *126*, 12684 – 12687.

[79] M. Murdoch, G. I. Waterhouse, M. A. Nadeem, J. B. Metson, M. A. Keane, R. F. Howe, J. Llorca, H. Idriss, *Nat. Chem.* **2011**, *3*, 489 – 492.

[80] P. Shen, S. Zhao, D. Su, Y. Li, A. Orlov, *Appl. Catal. B* **2012**, *126*, 153 – 160.

[81] Y. Xin, L. Wu, L. Ge, C. Han, Y. Li, S. Fang, *J. Mater. Chem. A* **2015**, *3*, 8659 – 8666.

[82] Z. Jiang, J. Zhu, D. Liu, W. Wei, J. Xie, M. Chen, *CrystEngComm* **2014**, *16*, 2384.

[83] a) M. Cargnello, M. Grzelczak, B. Rodriguez-Gonzalez, Z. Syrgiannis, K. Bakhmutsky, V. La Parola, L. M. Liz-Marzan, R. J. Gorte, M. Prato, P. Fornasiero, *J. Am. Chem. Soc.* **2012**, *134*, 11760 – 11766; b) M. Melchionna, A. Beltram, T. Montini, M. Monai, L. Nasi, P. Fornasiero, M. Prato, *Chem. Commun.* **2016**, *52*, 764 – 767.

[84] H. Zhou, J. Pan, L. Ding, Y. Tang, J. Ding, Q. Guo, T. Fan, D. Zhang, *Int. J. Hydrogen Energy* **2014**, *39*, 16293 – 16301.

[85] H. Hata, Y. Kobayashi, V. Bojan, W. J. Youngblood, *Nano Lett.* **2008**, *8*, 794 – 799.

[86] a) M. Cheng, M. Zhu, Y. Du, P. Yang, *Int. J. Hydrogen Energy* **2013**, *38*, 8631 – 8638; b) Y. Mizukoshi, K. Sato, T. J. Konno, N. Masahashi, *Appl. Catal. B* **2010**, *94*, 248 – 253.

[87] R. Su, M. M. Forde, Q. He, Y. Shen, X. Wang, N. Dimitratos, S. Wendt, Y. Huang, B. B. Iversen, C. J. Kiely, F. Besenbacher, G. J. Hutchings, *Dalton Trans.* **2014**, *43*, 14976 – 14982.

[88] J. Fang, L. Xu, Z. Zhang, Y. Yuan, S. Cao, Z. Wang, L. Yin, Y. Liao, C. Xue, *ACS Appl. Mater. Interfaces* **2013**, *5*, 8088 – 8092.

[89] J. Ran, J. Zhang, J. Yu, M. Jaroniec, S. Z. Qiao, *Chem. Soc. Rev.* **2014**, *43*, 7787 – 7812.

[90] L. Clarizia, D. Spasiano, I. Di Somma, R. Marotta, R. Andreozzi, D. D. Dionysiou, *Int. J. Hydrogen Energy* **2014**, *39*, 16812 – 16831.

[91] Q. Simon, D. Barreca, A. Gasparotto, C. Maccato, T. Montini, V. Gombac, P. Fornasiero, O. I. Lebedev, S. Turner, G. Van Tendeloo, *J. Mater. Chem.* **2012**, *22*, 11739.

[92] V. Gombac, L. Sordelli, T. Montini, J. J. Delgado, A. Adamski, G. Adami, M. Cargnello, S. Bernal, P. Fornasiero, *J. Phys. Chem. A* **2010**, *114*, 3916 – 3925.

[93] S. Obregón, M. J. Muñoz-Batista, M. Fernández-García, A. Kubacka, G. Colón, *Appl. Catal. B* **2015**, *179*, 468 – 478.

[94] X.-J. Lv, S.-X. Zhou, C. Zhang, H.-X. Chang, Y. Chen, W.-F. Fu, *J. Mater. Chem.* **2012**, *22*, 18542.

[95] W.-T. Chen, A. Chan, D. Sun-Waterhouse, T. Moriga, H. Idriss, G. I. N. Waterhouse, *J. Catal.* **2015**, *326*, 43 – 53.

[96] A. K. Agegnehu, C.-J. Pan, J. Rick, J.-F. Lee, W.-N. Su, B.-J. Hwang, *J. Mater. Chem.* **2012**, *22*, 13849.

[97] N. M. Mohamed, R. Bashiri, F. K. Chong, S. Sufian, S. Kakooei, *Int. J. Hydrogen Energy* **2015**, *40*, 14031 – 14038.

[98] T. R. Thurston, J. P. Wilcoxon, *J. Phys. Chem. B* **1999**, *103*, 11.

[99] X. Zong, H. Yan, G. Wu, G. Ma, F. Wen, L. Wang, C. Li, *J. Am. Chem. Soc.* **2008**, *130*, 7176 – 7177.

[100] X. Zong, G. Wu, H. Yan, G. Ma, J. Shi, F. Wen, L. Wang, C. Li, *J. Phys. Chem. C* **2010**, *114*, 1963 – 1968.

[101] L. Shen, M. Luo, Y. Liu, R. Liang, F. Jing, L. Wu, *Appl. Catal. B* **2015**, *166 – 167*, 445 – 453.

[102] Y. Hou, A. B. Laursen, J. Zhang, G. Zhang, Y. Zhu, X. Wang, S. Dahl, I. Chorkendorff, *Angew. Chem. Int. Ed.* **2013**, *52*, 3621 – 3625; *Angew. Chem.* **2013**, *125*, 3709 – 3713.

[103] Y.-J. Yuan, Z.-J. Ye, H.-W. Lu, B. Hu, Y.-H. Li, D.-Q. Chen, J.-S. Zhong, Z.-T. Yu, Z.-G. Zou, *ACS Catal.* **2016**, *6*, 532 – 541.

[104] Q. Xiang, J. Yu, M. Jaroniec, *J. Am. Chem. Soc.* **2012**, *134*, 6575 – 6578.

[105] a) S. Cao, Y. Chen, C.-C. Hou, X.-J. Lv, W.-F. Fu, *J. Mater. Chem. A* **2015**, *3*, 6096 – 6101; b) S. Cao, Y. Chen, C. J. Wang, P. He, W. F. Fu, *Chem. Commun.* **2014**, *50*, 10427 – 10429.

[106] J. F. Callejas, J. M. McEnaney, C. G. Read, J. C. Crompton, A. J. Biacchi, E. J. Popczun, T. R. Gordon, N. S. Lewis, R. E. Schaak, *ACS Nano* **2014**, *8*, 11101 – 11107.

[107] a) Y. Ma, X. Wang, Y. Jia, X. Chen, H. Han, C. Li, *Chem. Rev.* **2014**, *114*, 9987 – 10043; b) J. Schneider, M. Matsuoka, M. Takeuchi, J. Zhang, Y. Horiuchi, M. Anpo, D. W. Bahnemann, *Chem. Rev.* **2014**, *114*, 9919 – 9986.

[108] X. Chen, L. Liu, P. Y. Yu, S. S. Mao, *Science* **2011**, *331*, 746 – 750.

[109] a) J. Cai, Y. Zhu, D. Liu, M. Meng, Z. Hu, Z. Jiang, *ACS Catal.* **2015**, *5*, 1708 – 1716; b) Z. Wang, C. Yang, T. Lin, H. Yin, P. Chen, D. Wan, F. Xu, F. Huang, J. Lin, X. Xie, M. Jiang, *Adv. Funct. Mater.* **2013**, *23*, 5444 – 5450; c) A. Naldoni, M. Allieta, S. Santangelo, M. Marelli, F. Fabbri, S. Cappelli, C. L. Bianchi, R. Psaro, V. Dal Santo, *J. Am. Chem. Soc.* **2012**, *134*, 7600 – 7603; d) Y. Zhu, D. Liu, M. Meng, *Chem. Commun.* **2014**, *50*, 6049 – 6051.

[110] X. Yu, B. Kim, Y. K. Kim, *ACS Catal.* **2013**, *3*, 2479 – 2486.

[111] A. Sinhamahapatra, J.-P. Jeon, J.-S. Yu, *Energy Environ. Sci.* **2015**, *8*, 3539 – 3544.

[112] Q. Tay, X. Liu, Y. Tang, Z. Jiang, T. C. Sum, Z. Chen, *J. Phys. Chem. C* **2013**, *117*, 14973 – 14982.

[113] a) T. Sun, E. Liu, X. Liang, X. Hu, J. Fan, *Appl. Surf. Sci.* **2015**, *347*, 696 – 705; b) S. Taylor, M. Mehta, A. Samokhvalov, *ChemPhysChem* **2014**, *15*, 942 – 949; c) D. Y. Leung, X. Fu, C. Wang, M. Ni, M. K. Leung, X. Wang, X. Fu, *ChemSusChem* **2010**, *3*, 681 – 694.

[114] N. Manfredi, B. Cecconi, V. Calabrese, A. Minotti, F. Peri, R. Ruffo, M. Monai, I. Romero-Ocana, T. Montini, P. Fornasiero, A. Abbotto, *Chem. Commun.* **2016**, *52*, 6977 – 6980.

[115] a) D. Duonghong, E. Borgarello, M. Grätzel, *J. Am. Chem. Soc.* **1981**, *103*, 4685 – 4690; b) K. Hirano, E. Suzuki, A. Ishikawa, T. Moroi, H. Shiroishi, M. Kaneko, *J. Photochem. Photobiol. A* **2000**, *136*, 157 – 161.

[116] a) H. Park, W. Choi, M. R. Hoffmann, *J. Mater. Chem.* **2008**, *18*, 2379; b) A. M. Hussein, R. V. Shende, *Int. J. Hydrogen Energy* **2014**, *39*, 5557 – 5568; c) R. Sasikala, A. Shirole, V. Sudarsan, T. Sakuntala, C. Sudakar, R. Naik, S. R. Bharadwaj, *Int. J. Hydrogen Energy* **2009**, *34*, 3621 – 3630; d) Z. Wang, Y. Liu, D. J. Martin, W. Wang, J. Tang, W. Huang, *Phys. Chem. Chem. Phys.* **2013**, *15*, 14956 – 14960.

[117] a) L. Amirav, A. P. Alivisatos, *J. Phys. Chem. Lett.* **2010**, *1*, 1051 – 1054; b) W. Zhang, Y. Wang, Z. Wang, Z. Zhong, R. Xu, *Chem. Commun.* **2010**, *46*, 7631 – 7633; c) L.-X. Hao, G. Chen, Y.-G. Yu, Y.-S. Zhou, Z.-H. Han, Y. Liu, *Int. J. Hydrogen Energy* **2014**, *39*, 14479 – 14486.

[118] a) P. Zhang, T. Wang, J. Gong, *Adv. Mater.* **2015**, *27*, 5328 – 5342; b) S. Linic, P. Christopher, D. B. Ingram, *Nat. Mater.* **2011**, *10*, 911 – 921.

[119] P. Christopher, H. Xin, S. Linic, *Nat. Chem.* **2011**, *3*, 467 – 472.

[120] a) Y. Shiraishi, D. Tsukamoto, Y. Sugano, A. Shiro, S. Ichikawa, S. Tanaka, T. Hirai, *ACS Catal.* **2012**, *2*, 1984 – 1992; b) W. Zhai, S. Xue, A. Zhu, Y. Luo, Y. Tian, *ChemCatChem* **2011**, *3*, 127 – 130.

[121] R. Li, W. Chen, H. Kobayashi, C. Ma, *Green Chem.* **2010**, *12*, 212 – 215.

[122] D. P. Sahoo, S. Patnaik, D. Rath, B. Nanda, K. Parida, *RSC Adv.* **2016**, *6*, 112602 – 112613.

[123] T. Tana, X. W. Guo, Q. Xiao, Y. Huang, S. Sarina, P. Christopher, J. Jia, H. Wu, H. Zhu, *Chem. Commun.* **2016**, *52*, 11567 – 11570.

[124] N. Zhang, C. Han, Y.-J. Xu, J. J. Foley IV, D. Zhang, J. Codrington, S. K. Gray, Y. Sun, *Nat. Photonics* **2016**, *10*, 473 – 482.

[125] a) O. Rosseler, M. V. Shankar, M. K.-L. Du, L. Schmidlin, N. Keller, V. Keller, *J. Catal.* **2010**, *269*, 179 – 190; b) J. Zhang, Q. Xu, Z. Feng, M. Li, C. Li, *Angew. Chem. Int. Ed.* **2008**, *47*, 1766 – 1769; *Angew. Chem.* **2008**, *120*, 1790 – 1793; c) Y. K. Kho, A. Iwase, W. Y. Teoh, L. Ma, R. Amal, *J. Phys. Chem. C* **2010**, *114*, 2821 – 2829; d) Q. Xu, Y. Ma, J. Zhang, X. Wang, Z. Feng, C. Li, *J. Catal.* **2011**, *278*, 329 – 335.

[126] L. Huang, X. Wang, J. Yang, G. Liu, J. Han, C. Li, *J. Phys. Chem. C* **2013**, *117*, 11584 – 11591.

[127] G. Carraro, A. Gasparotto, C. Maccato, V. Gombac, F. Rossi, T. Montini, D. Peeters, E. Bontempi, C. Sada, D. Barreca, P. Fornasiero, *RSC Adv.* **2014**, *4*, 32174.

[128] Y. Wang, Z. Zhang, Y. Zhu, Z. Li, R. Vajtai, L. Ci, P. M. Ajayan, *ACS Nano* **2008**, *2*, 1492 – 1496.

[129] D. Barreca, P. Fornasiero, A. Gasparotto, V. Gombac, C. Maccato, T. Montini, E. Tondello, *ChemSusChem* **2009**, *2*, 230 – 233.

[130] A. Gasparotto, D. Barreca, D. Bekermann, A. Devi, R. A. Fischer, P. Fornasiero, V. Gombac, O. I. Lebedev, C. Maccato, T. Montini, G. Van Tendeloo, E. Tondello, *J. Am. Chem. Soc.* **2011**, *133*, 19362 – 19365.

[131] L. Ma, H. Fan, J. Wang, Y. Zhao, H. Tian, G. Dong, *Appl. Catal. B* **2016**, *190*, 93 – 102.
[132] a) J. Zhang, Y. Chen, X. Wang, *Energy Environ. Sci.* **2015**, *8*, 3092 – 3108; b) S. Cao, J. Yu, *J. Phys. Chem. Lett.* **2014**, *5*, 2101 – 2107; c) W. J. Ong, L. L. Tan, Y. H. Ng, S. T. Yong, S. P. Chai, *Chem. Rev.* **2016**, *116*, 7159 – 7329.
[133] D. J. Martin, K. Qiu, S. A. Shevlin, A. D. Handoko, X. Chen, Z. Guo, J. Tang, *Angew. Chem. Int. Ed.* **2014**, *53*, 9240 – 9245; *Angew. Chem.* **2014**, *126*, 9394 – 9399.
[134] P. Niu, L. Zhang, G. Liu, H.-M. Cheng, *Adv. Funct. Mater.* **2012**, *22*, 4763 – 4770.
[135] Y. Chen, B. Wang, S. Lin, Y. Zhang, X. Wang, *J. Phys. Chem. C* **2014**, *118*, 29981 – 29989.
[136] W. Ho, Z. Zhang, M. Xu, X. Zhang, X. Wang, Y. Huang, *Appl. Catal. B* **2015**, *179*, 106 – 112.
[137] Y. Kang, Y. Yang, L. C. Yin, X. Kang, G. Liu, H. M. Cheng, *Adv. Mater.* **2015**, *27*, 4572 – 4577.
[138] K. C. Christoforidis, A. Iglesias-Juez, S. J. Figueroa, M. A. Newton, M. Di Michiel, M. Fernandez-Garcia, *Phys. Chem. Chem. Phys.* **2012**, *14*, 5628 – 5634.
[139] V. W. Lau, M. B. Mesch, V. Duppel, V. Blum, J. Senker, B. V. Lotsch, *J. Am. Chem. Soc.* **2015**, *137*, 1064 – 1072.
[140] Y. Cui, G. Zhang, Z. Lin, X. Wang, *Appl. Catal. B* **2016**, *181*, 413 – 419.
[141] Q. Liang, Z. Li, Z.-H. Huang, F. Kang, Q.-H. Yang, *Adv. Funct. Mater.* **2015**, *25*, 6885 – 6892.
[142] J. Zhang, M. Zhang, R. Q. Sun, X. Wang, *Angew. Chem. Int. Ed.* **2012**, *51*, 10145 – 10149; *Angew. Chem.* **2012**, *124*, 10292 – 10296.
[143] Z. Huang, F. Li, B. Chen, G. Yuan, *ChemSusChem* **2016**, *9*, 478 – 484.
[144] J. Liu, J. Huang, H. Zhou, M. Antonietti, *ACS Appl. Mater. Interfaces* **2014**, *6*, 8434 – 8440.
[145] a) Y. Zhao, F. Zhao, X. Wang, C. Xu, Z. Zhang, G. Shi, L. Qu, *Angew. Chem. Int. Ed.* **2014**, *53*, 13934 – 13939; *Angew. Chem.* **2014**, *126*, 14154 – 14159; b) Y. Cui, J. Zhang, G. Zhang, J. Huang, P. Liu, M. Antonietti, X. Wang, *J. Mater. Chem.* **2011**, *21*, 13032.
[146] a) M. K. Bhunia, K. Yamauchi, K. Takanabe, *Angew. Chem. Int. Ed.* **2014**, *53*, 11001 – 11005; *Angew. Chem.* **2014**, *126*, 11181 – 11185; b) Z. P. Chen, M. Antonietti, D. Dontsova, *Chem. Eur. J.* **2015**, *21*, 10805 – 10811.
[147] a) L. Ge, F. Zuo, J. Liu, Q. Ma, C. Wang, D. Sun, L. Bartels, P. Feng, *J. Phys. Chem. C* **2012**, *116*, 13708 – 13714; b) D. Zheng, C. Pang, X. Wang, *Chem. Commun.* **2015**, *51*, 17467 – 17470; c) Y. Di, X. Wang, A. Thomas, M. Antonietti, *ChemCatChem* **2010**, *2*, 834 – 838; d) Z. Li, Y. Wu, G. Lu, *Appl. Catal. B* **2016**, *188*, 56 – 64.
[148] L. Ge, C. Han, *Appl. Catal. B* **2012**, *117 – 118*, 268 – 274.
[149] J. Wang, J. Huang, H. Xie, A. Qu, *Int. J. Hydrogen Energy* **2014**, *39*, 6354 – 6363.
[150] S. Obregón, G. Colón, *Appl. Catal. B* **2014**, *144*, 775 – 782.
[151] M. Li, L. Zhang, X. Fan, M. Wu, Y. Du, M. Wang, Q. Kong, L. Zhang, J. Shi, *Appl. Catal. B* **2016**, *190*, 36 – 43.
[152] a) J.-P. Zou, L.-C. Wang, J. Luo, Y.-C. Nie, Q.-J. Xing, X.-B. Luo, H.-M. Du, S.-L. Luo, S. L. Suib, *Appl. Catal. B* **2016**, *193*, 103 – 109; b) Y. Chen, J. Li, Z. Hong, B. Shen, B. Lin, B. Gao, *Phys. Chem. Chem. Phys.* **2014**, *16*, 8106 – 8113; c) A. Suryawanshi, P. Dhanasekaran, D. Mhamane, S. Kelkar, S. Patil, N. Gupta, S. Ogale, *Int. J. Hydrogen Energy* **2012**, *37*, 9584 – 9589; d) Y. Zhong, J. Yuan, J. Wen, X. Li, Y. Xu, W. Liu, S. Zhang, Y. Fang, *Dalton Trans.* **2015**, *44*, 18260 – 18269; e) J. Zhang, M. Zhang, L. Lin, X. Wang, *Angew. Chem. Int. Ed.* **2015**, *54*, 6297 – 6301; *Angew. Chem.* **2015**, *127*, 6395 – 6399.
[153] J. Liu, Y. Liu, N. Liu, Y. Han, X. Zhang, H. Huang, Y. Lifshitz, S.-T. Lee, J. Zhong, Z. Kang, *Science* **2015**, *347*, 970 – 974.
[154] a) M. Melchionna, M. Prato, P. Fornasiero, *Catal. Today* **2016**, *277*, 202 – 213; b) N. Zhang, M. Q. Yang, S. Liu, Y. Sun, Y. J. Xu, *Chem. Rev.* **2015**, *115*, 10307 – 10377.
[155] Q. Xiang, J. Yu, M. Jaroniec, *Chem. Soc. Rev.* **2012**, *41*, 782 – 796.
[156] S. Sakthivel, H. Kisch, *Angew. Chem. Int. Ed.* **2003**, *42*, 4908 – 4911; *Angew. Chem.* **2003**, *115*, 5057 – 5060.
[157] K. C. Christoforidis, T. Montini, E. Bontempi, S. Zafeiratos, J. J. D. Jaén, P. Fornasiero, *Appl. Catal. B* **2016**, *187*, 171 – 180.
[158] Q. Li, B. Guo, J. Yu, J. Ran, B. Zhang, H. Yan, J. R. Gong, *J. Am. Chem. Soc.* **2011**, *133*, 10878 – 10884.
[159] Y. Li, H. Wang, S. Peng, *J. Phys. Chem. C* **2014**, *118*, 19842 – 19848.
[160] X.-J. Lv, W.-F. Fu, H.-X. Chang, H. Zhang, J.-S. Cheng, G.-J. Zhang, Y. Song, C.-Y. Hu, J.-H. Li, *J. Mater. Chem.* **2012**, *22*, 1539 – 1546.
[161] Z. Sun, J. Guo, S. Zhu, L. Mao, J. Ma, D. Zhang, *Nanoscale* **2014**, *6*, 2186 – 2193.
[162] W. Fan, Q. Lai, Q. Zhang, Y. Wang, *J. Phys. Chem. C* **2011**, *115*, 10694 – 10701.
[163] L. Ye, J. Fu, Z. Xu, R. Yuan, Z. Li, *ACS Appl. Mater. Interfaces* **2014**, *6*, 3483 – 3490.
[164] Y. Yang, E. Liu, H. Dai, L. Kang, H. Wu, J. Fan, X. Hu, H. Liu, *Int. J. Hydrogen Energy* **2014**, *39*, 7664 – 7671.
[165] H.-i. Kim, G.-h. Moon, D. Monllor-Satoca, Y. Park, W. Choi, *J. Phys. Chem. C* **2012**, *116*, 1535 – 1543.
[166] J. Xu, L. Zhang, R. Shi, Y. Zhu, *J. Mater. Chem. A* **2013**, *1*, 14766.
[167] B. Chai, T. Peng, J. Mao, K. Li, L. Zan, *Phys. Chem. Chem. Phys.* **2012**, *14*, 16745 – 16752.
[168] P. Gao, J. Liu, S. Lee, T. Zhang, D. D. Sun, *J. Mater. Chem.* **2012**, *22*, 2292 – 2298.
[169] W. Kang, X. Jimeng, W. Xitao, *Appl. Surf. Sci.* **2016**, *360*, 270 – 275.
[170] H. W. Jeong, H. Park, *Catal. Today* **2014**, *230*, 15 – 19.
[171] X. Wang, R. Lv, K. Wang, *J. Mater. Chem. A* **2014**, *2*, 8304 – 8313.
[172] Q. Li, L. Chen, G. Lu, *J. Phys. Chem. C* **2007**, *111*, 11494 – 11499.
[173] a) D. Wang, J. Huang, K. Li, C. Zhang, Y. Du, P. Yang, *RSC Adv.* **2016**, *6*, 34699 – 34707; b) J. Huang, D. Wang, Z. Yue, X. Li, D. Chu, P. Yang, *J. Phys. Chem. C* **2015**, *119*, 27892 – 27899.

Manuscript received: December 19, 2016
Revised: January 20, 2017
Accepted Article published: January 24, 2017
Final Article published: March 27, 2017